

A Set-Valued Approach to FDI and FTC of Wind Turbines

Pedro Casau, Paulo Rosa, Seyed Mojtaba Tabatabaeipour, Carlos Silvestre, and Jakob Stoustrup, *Senior Member, IEEE*

Abstract—A complete methodology to design robust fault detection and isolation (FDI) filters and fault-tolerant control (FTC) schemes for linear parameter varying systems is proposed, with particular focus on its applicability to wind turbines. This paper takes advantage of the recent advances in model falsification using set-valued observers (SVOs) that led to the development of FDI methods for uncertain linear time-varying systems, with promising results in terms of the time required to diagnose faults. An integration of such SVO-based FDI methods with robust control synthesis is described, to deploy new FTC algorithms that are able to stabilize the plant under faulty environments. The FDI and FTC algorithms are assessed by resorting to a publicly available wind turbine benchmark model, using Monte Carlo simulation runs.

Index Terms—Fault detection, fault diagnosis, fault tolerant systems, wind energy.

I. INTRODUCTION

THE development of wind energy conversion systems has been growing steadily over the last few decades and it is expected to keep this pace over the years to come. However, the construction and maintenance of on-shore/off-shore wind turbines is very capital intensive and their inoperative situations should be kept minimal to ensure economic viability. Such evidence fueled the research of fault detection and isolation (FDI) algorithms and their application to wind turbines, which constitutes the main focus of this paper. The implementation of these techniques yields several advantages, including:

- 1) avoidance of premature breakdown;
- 2) reduction of maintenance costs;

Manuscript received April 30, 2013; revised October 1, 2013 and January 16, 2014; accepted April 3, 2014. Date of publication June 5, 2014; date of current version December 15, 2014. Manuscript received in final form May 4, 2014. The work of P. Casau was supported by the Fundação para a Ciência e a Tecnologia under Grant SFRH/BD/70656/2010. Recommended by Associate Editor N. E. Wu.

P. Casau is with the Institute for Systems and Robotics–Instituto Superior Técnico, Lisbon 1049-001, Portugal (e-mail: pcasau@isr.ist.utl.pt).

P. Rosa is with Deimos Engenharia, Lisbon 1998-023, Portugal (e-mail: paulo.rosa@deimos.com.pt).

S. M. Tabatabaeipour is with the Automation and Control Group, Department of Electrical Engineering, Technical University of Denmark, Kgs. Lyngby DK 2800, Denmark (e-mail: setaba@elektro.dtu.dk).

C. Silvestre is with the Institute for Systems and Robotics–Instituto Superior Técnico, Lisbon 1049-001, Portugal, and also with the Department of Electrical and Computer Engineering, Faculty of Science and Technology, University of Macau, Taipa, Macau (e-mail: cjs@isr.ist.utl.pt).

J. Stoustrup is with Aalborg University, Aalborg 9220, Denmark (e-mail: jakob@es.aau.dk).

Color versions of one or more of the figures in this paper are available online at <http://ieeexplore.ieee.org>.

Digital Object Identifier 10.1109/TCST.2014.2322777

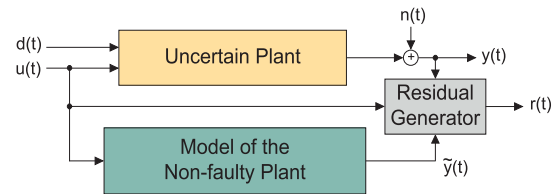


Fig. 1. Residual generation in a classical FD architecture.

- 3) remote diagnosis;
- 4) improvement of the capacity factor;¹
- 5) support for future wind turbine development [2].

However, wind farm monitoring still relies on the decisions of a human operator or on practical knowledge from experienced staff. New condition monitoring systems (CMS) and fault detection systems (FDS) tend to be driven toward fully autonomous operation. Some algorithms which are still under intensive research include:

- 1) parameter estimation methods;
- 2) observer-based methods;
- 3) knowledge-based expert systems;
- 4) learning agents [2].

This article discusses the application of a novel observer-based algorithm to the FDI of wind turbines.

The field of FDI algorithms has been studied since the early 1970s [3], and several techniques have, since then, been applied to different types of systems. Common examples of systems equipped with FDI devices include aircrafts and a wide range of industrial processes such as the ones described in [4]–[9]. An FDI system must be able to withstand different types of faults in the sensors and/or actuators. These faults can occur abruptly or slowly in time. Moreover, model uncertainty (such as unmodeled dynamics) and disturbances must never be interpreted as faults.

A deterministic model-based FDS is usually composed of two parts: a filter that generates residuals which should become large under faulty environments (see Fig. 1); and a decision threshold, which is used to decide whether a fault is present or not (see [3], [5], and [10]–[13], and references therein). The isolation of the fault can, in some cases, be done using a similar approach, that is, by designing filters for families of faults, and identifying the most likely fault as that associated to the filter with the smallest residuals.

¹The capacity factor is the ratio between the actual power delivered during a time period and the power that would have been produced had the generator been operating at its full capacity [1].

The main idea in such architectures stems from the design of filters that are more sensitive to faults than to disturbances and model uncertainty. This can be achieved, for instance, by using geometric considerations regarding the plant, as in [9], [14], and [15], or by optimizing a particular norm minimization objective, such as the \mathcal{H}_∞ - or l_1 -norm (see [6], [8], and [16]–[18]). The latter approach provides, in general, important robustness properties, as stressed in [5], [7], [16], and [19], by explicitly accounting for model uncertainty. In [20], integral quadratic constraints for uncertain systems are used for model validation. As a caveat, these methodologies are, in general, conservative or can only be applied to a restricted class of systems. Moreover, the thresholds used to declare faults are typically time-varying and highly dependent on the model uncertainty and on the amplitude of the exogenous disturbances and measurement noise.

The FDI strategy proposed in this paper uses a different philosophy. Rather than identifying the most likely model of the faulty plant, models that are not compatible with the current input/output data are invalidated, thus avoiding the computation of decision thresholds. To this end, this paper adopts the model falsification technique using set-valued observers (SVOs) described in Section III. In addition, another advantage of the SVO-based methodology presented herein stems from the fact that it is able to deal with linear parameter varying (LPV) uncertain plants. Alternative set-membership approaches to FDI can be found in [21] and [22], and references therein, and will be briefly discussed in Section IV.

The use of FDI strategies, however, may not completely void the possibility of having severe failures that, due to delay in the corresponding isolation process, lead to the damage of the diagnosed system beyond repair. Therefore, control design methodologies that take into account these considerations have been developed in the recent years. By increasing the detectability of certain faults using input design methods, one might be able to respond more rapidly to failures. As an example, nested controller and FDI design strategies [18], [23], [24] have been proposed that allow faster detection of the faults owing to a poorer rejection of the controller with respect to disturbances aligned with these faults. As a shortcoming, the lack of attenuation of the faults can put into jeopardy the entire system. Once a fault is isolated, the controller can be reconfigured to minimize its impact on the performance of the closed-loop system. Such architectures are typically referred to as active fault-tolerant control (AFTC) schemes. In [25], an active fault detection (FD) method was proposed where excitation signals are designed to guarantee detection and isolation of faults when set-valued estimations of states are obtained based on SVOs.

The main contributions of this article are as follows.

- 1) A thorough description of an SVO-based FDI and FTC methodology.
- 2) The application of the aforementioned technique to FDI and FTC of wind turbines.
- 3) The evaluation of the proposed strategy using simulations of the benchmark model described in [26].
- 4) The design of a controller which is robust to variations on the parameters of the system plant.

A preliminary version of this paper, without the detailed analysis on the SVO strategy that is carried out in this paper, may be found in [27].

The remainder of this paper is organized as follows. Section II introduces the main notation used throughout the paper, while Section III describes the main concepts regarding model falsification. SVOs for LPV systems are presented in Section IV, and some of the main issues that appear in the implementation of this type of filters are discussed. These SVOs are used in Section V for FDI and FTC, while in Section VIII a brief description of the application of this methodology to a wind turbine is shown. Finally, Section IX is devoted to the discussion of the proposed approach.

II. PRELIMINARIES AND NOTATION

We represent the elements of $v(k) \in \mathbb{R}^m$, for some m , $k \in \mathbb{Z}$, $m > 0$, as $v_i(k)$, so that $v(k) = [v_1(k), \dots, v_m(k)]^T$. The concatenation of vectors $v(k)$, $v(k-1)$, \dots , $v(k-N+1)$, for $N \in \mathbb{Z}^+$ is denoted as $v_N = [v(k), \dots, v(k-N+1)]^T$. For the sake of simplicity, v is used instead of v_N whenever N can be inferred from the context. We assume that the available input/output data set can be obtained through a LPV system, described by

$$\begin{aligned} x(k+1) &= A(\phi(k))x(k) + B_u(\phi(k))u(k) + L(\phi(k))d(k) \\ y(k) &= C(\phi(k))x(k) + H(\phi(k))n(k) \end{aligned} \quad (1)$$

with bounded exogenous disturbances, $d(\cdot)$, uncertain initial state, $x(0) \in X(0) \subset \mathbb{R}^{n_x}$, control input, $u(\cdot)$, and measurement output, $y(\cdot)$, corrupted by additive noise, $n(\cdot)$. The matrices of the system may be uncertain and are assumed to depend upon a (partially uncertain) time-varying vector of parameters, $\phi(\cdot)$. It is also assumed that $|d(k)| = \max_i |d_i(k)| \leq 1$, and $|n(k)| \leq \bar{n}$. At each time, k , let $x(k)$ denote the states vector and $X(k) = \text{Set}(M(k), m(k))$, where

$$\text{Set}(M, m) = \{q \in \mathbb{R}^n : Mq \leq m\} \quad (2)$$

represents a convex polytope, with $M(k) \in \mathbb{R}^{n_m \times n}$, $m(k) \in \mathbb{R}^{n_m}$, and with the inequality taken elementwise. Moreover, let $x(k) \in \mathbb{R}^{n_x}$, $d(k) \in \mathbb{R}^{n_d}$, $u(k) \in \mathbb{R}^{n_u}$, and $y(k) \in \mathbb{R}^{n_y}$, for $k \geq 0$.

Remark 1: It is not assumed that the trajectory of the vector of parameters, ϕ , is known as a *priori*. In fact, at each time, k , the vector $\phi(k)$ (or part of it) is measured. Moreover, ϕ might be used to encode information about system faults. \diamond

III. MODEL FALSIFICATION

The problem of model falsification appears in several areas where we are interested in distinguishing among an eligible set of dynamic systems. The simplest model falsification problem one can think of is that of stating whether or not a given dynamic model is compatible with the current observed input/output data. However, it is important to notice that a model can never be validated in practice. Indeed, if the model is compatible with the input/output data up to time t , it need not be compatible at time $t + \delta$, where $\delta > 0$.

Therefore, one can only say that a given model is not falsified (or invalidated) by the current input/output data. On the other hand, a model is obviously invalidated or falsified once it is not compatible with the observations. Hence, we usually refer to model falsification rather than model validation, since the latter is not achievable in practice.

As an example, suppose that there are four possible models, M_1 , M_2 , M_3 , and M_4 , for a given plant. We are interested in deciding which model (if any) is able to explain the input/output data sequence that we are obtaining from the sensors and actuators' commands. Therefore, assume that, at a given initial time t_0 , all the four models are plausible. Further suppose that, at time t_1 , model M_4 is invalidated, that is, the sensors readings cannot be explained by model M_4 . Moreover, consider that, at time t_2 , model M_2 is invalidated and that, finally, model M_1 is invalidated at time t_3 . Then, at time t_3 , we conclude that the only model capable of explaining the input/output time-series generated by the plant is model M_3 .

Unmodeled dynamics (present in virtually every physical system) and adverse exogenous disturbances, can result in erroneous model falsification. Therefore, worst case approaches, rather than stochastic approaches, are more suitable to address this type of problems. In fact, the solution proposed in [28] for uncertain LTI systems, and later on extended to linear time-varying (LTV) systems in [29], assumes that the system is described by an LTI nominal model interconnected with an LTI or LTV unknown system, denoted by Δ . This uncertain system Δ can be used, for instance, to describe unmodeled dynamics and parametric uncertainty. However, the methods provided in [28] and [29] are not recursive, which means that, after a given amount of input/output data is obtained, we check whether or not it is compatible with the model of the system. Hence, the complexity of the algorithm grows with the number of iterations.

The model falsification strategy presented in this paper uses a philosophy similar to that of [28] and [29], but proposes a recursive algorithm. As shown in the following section, this method guarantees that valid models of the plant are never falsified. Moreover, under certain distinguishability conditions discussed herein, it is also shown that the correct model of the plant is selected.

A. (In)Distinguishability Problem

Because of noise and uncertainty on the model of the system, it is possible that an input/output sequence is consistent with more than one model. In such circumstances, we cannot distinguish the correct one among a set of plausible models of the plant. A remedy to this is to use active diagnosis methods to improve the distinguishability between valid models by exciting the system using an auxiliary input signal. In active diagnosis, the diagnoser generates an input that excites the system, to decide whether the output represents a normal or a faulty behavior and, if possible, decide which fault has occurred. The generated input must perturb the system from the operation point but, at the same time, not lead the system to instability or to an unacceptable

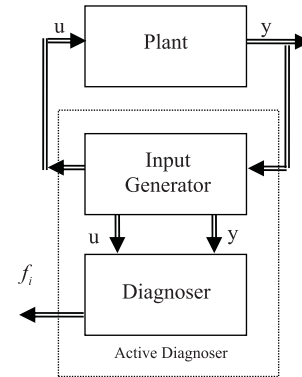


Fig. 2. Structure of an active fault diagnoser.

performance. The area of active diagnosis has attracted a considerable attention in recent years (see [30]–[34], and references therein).

The structure of an active diagnoser is shown in Fig. 2, consisting of an input generator and a diagnoser. The input generator produces an input sequence $U = [u(0), \dots, u(N_d - 1)]$ which is applied to the system. The occurrence of a fault f is determined by the diagnoser by observing the applied input sequence and the output sequence $Y = [y(0), \dots, y(N_d)]$, where $\{0, \dots, N_d\} \subset \mathbb{N}_0$ is the time horizon over which we test for distinguishability.

The active diagnosis problem can be stated as follows.

Problem 1 (Active Diagnosis Problem): Given the set of system models $\mathcal{M} = \{M_0, \dots, M_{N_M}\}$ describing behaviors of the system with no fault and subject to faults $\{f_1, \dots, f_{N_M}\}$, respectively, find a sequence of inputs U such that (U, Y) can only be described by a unique M_i . \square

In other words, the set \mathcal{M} must be distinguishable. If, in addition, there exists $N_d > 0$ such that there exist a unique M_i which describes (U, Y) for $\{0, 1, \dots, N_d\}$ then the system is said to be distinguishable in N_d sampling times (see [35]). The problem can be formulated as a feasibility test problem as follows:

$$\begin{aligned}
 & \text{find } N_d, u \text{ such that} \\
 & \overbrace{\begin{aligned}
 x_i(k+1) &= A_i(\phi(k))x_i(k) + B_{u_i}(\phi(k))u(k) + L_i(\phi(k))d(k) \\
 y_i(k) &= C_i(\phi(k))x_i(k) + H_i(\phi(k))n(k) \\
 y_i(N_d) - y_j(N_d) &\neq 0, \quad i, j \in \{0, \dots, N_M\}, i \neq j \\
 |n(k)| &\leq \bar{n}, \quad |d(k)| \leq 1, \quad x_i(0) \in X_i(0) \\
 k &= 0, \dots, N_d.
 \end{aligned}} \quad (3)
 \end{aligned}$$

Since this problem is in general nonconvex, we perform a slight modification that allows us to recast the feasibility problem as a convex problem. We assume that the general form of the auxiliary input signal is given as a periodic signal of the form $u(k) = a \sin(\omega k)$, with parameters a and ω —the applicability of this tool will be illustrated in Section VIII. The problem is to find the appropriate amplitude a and the frequency ω of the input signal that guarantees distinguishability of the corresponding outputs despite noise and disturbance. For a given a_0 and ω_0 , N_{d_0} , if there exist noise and disturbance sequences and initial condition such that

the following problem is feasible, then we cannot guarantee that the models are distinguishable:

$$\overbrace{\begin{aligned} & \text{test feasibility of} \\ & u(k) = a_0 \sin(\omega_0 k) \\ & x_i(k+1) = A_i(\phi(k))x_i(k) + B_{u_i}(\phi(k))u(k) + L_i(\phi(k))d(k) \\ & y_i(k) = C_i(\phi(k))x_i(k) + H_i(\phi(k))n(k) \\ & y_i(N_{d_0}) - y_j(N_{d_0}) = 0, \quad i, j \in \{0, \dots, N_M\}, i \neq j \\ & |n(k)| \leq \bar{n}, |d(k)| \leq 1, x_i(0) \in X_i(0). \end{aligned}} \quad (4)$$

Now, to solve (3) we look for a_0 , ω_0 , N_{d_0} that render (4) infeasible. Therefore, we parameterize (4) over a_0 , ω_0 , and N_{d_0} , using an appropriate gridding of the parameter range and check the feasibility of (4) at each grid point. The optimal signal can be found by choosing the optimal value of the parameter vector that makes (4) infeasible. The proposed method yields solving a finite number of linear programming problems that, for a reasonable grid density, is computationally efficient.

The strategy of designing input signals so as to enhance fault detectability, is usually referred to as active fault diagnosis and, even though we select a very simple sinusoidal signal as the input injection term, there are many other strategies available in the literature that achieve the same goal, namely [24] and [33], just to name a few. For the sake of completeness, let us highlight some differences to the work in [24] which also makes use of sinusoidal input excitation:

- 1) we do not impose any probabilistic model on the noise/disturbance signals but we do assume that the noise is bounded;
- 2) our strategy provides guarantees of distinguishability between two distinct models of the system while [24] such guarantee is not provided;
- 3) as a drawback, overbounding of the noise signal might result in very conservative estimates of distinguishability.

IV. SET-VALUED OBSERVERS

A. Introduction

If a dynamic model is not able to explain the output of the actual system, given the applied control inputs and bounds on the exogenous disturbances, it is straightforward to conclude that such a model is not compatible with the actual dynamics of the plant. Hence, this section is devoted to the description of a technique that allows one to systematically design filters, which, in turn, are going to be used for model falsification. These filters are referred to as SVOs (see [33]–[39], and references therein for an overview on SVOs) as they are able to provide set-valued estimates of the state of the plant, based upon:

- 1) the dynamic model of the system (which may be uncertain);
- 2) the output measurements;
- 3) the control inputs;
- 4) the bounds on the exogenous disturbances and measurement noise.

This type of observers, jointly with the model falsification paradigm described in the previous section, naturally arises as a solution to distinguish among models of dynamic systems. The problem of designing SVOs—also referred to as set-membership filtering design—has been extensively studied in the literature. One of the first algorithms developed to compute (ellipsoidal) set-valued estimates of the state of a system was introduced in [37] and [38]. In [40], an approach to the synthesis problem of SVOs for LTV plants with nonlinear equality constraints is described. A method for active mode observation of switching systems, based on SVOs, has been recently proposed in [41]. Zonotope-based approaches to FD were also recently proposed in [21] and [22]. The SVO-based methodology adopted in this paper is an extension of the work in [42]. In fact, the results in [43] are a generalization of the set-valued state estimation for LTV systems to set valued estimation for LPV systems, thus being able to handle model uncertainty. Indeed, this section briefly describes how to design SVOs that are able to provide set-valued estimates of the state, under different scenarios, namely parametric uncertainty in the input, output or matrices of the dynamics of the state-space representation of the plant. The proposed method is, in general, less computationally demanding when compared to zonotope-based approaches. The SVOs' prediction cycle consists in estimating the set of possible states, $\tilde{X}(k+1)$, at time $k+1$, based upon the model of the system and the set-valued estimate of the state at time k . The update cycle comprises the computation of the states, $Y(k+1)$, which are compatible with the measured output of the plant, and the intersection of this set with $\tilde{X}(k+1)$.

B. SVOs for LPV Dynamic Models

For completeness, some of the results described in [43] and [44] will also be presented in this article, as they are a fundamental part of the methodology adopted herein to design the FDI system.

Let $X(k+1)$ represent the set of possible states at time $k+1$, that is, the state $x(k+1)$ satisfies (1) with $x(k) \in X(k)$ if and only if $x(k+1) \in X(k+1)$. The goal of an SVO is to find $X(k+1)$, based upon (1) and with the additional knowledge that $x(k) \in X(k)$, $x(k-1) \in X(k-1)$, \dots , $x(k-N) \in X(k-N)$ for some finite horizon N . We further require that for all $x \in X(k+1)$, there exists $x^* \in X(k)$ such that, for $x(k) = x^*$, the observations are compatible with (1). In other words, we want $X(k+1)$ to be the smallest set containing all the solutions to (1). The computation of $X(k+1)$ based upon $X(k)$ for systems with no model uncertainty can be performed using the technique described in [42]. Indeed, let the system be described by (1), and assume that the matrices of the dynamics are exactly known. For the sake of simplicity, assume that $H(\phi(k)) = I$ for all $\phi(k)$, $k \geq 0$. Then, as shown in [42], $x(k+1) \in X(k+1)$ if and only if there exist $x(k)$, $n(k)$ and $d(k)$, such that, for the current measurement, $y(k+1)$, we have

$$P(k)[x(k+1)^T, x(k)^T, d(k)^T]^T \leq p(k) \quad (5)$$

where

$$P(k) = \begin{bmatrix} I & -A(\phi(k)) & -L(\phi(k)) \\ -I & A(\phi(k)) & L(\phi(k)) \\ 0 & 0 & I \\ 0 & 0 & -I \\ \tilde{M}(k) & 0 & 0 \\ 0 & M(k-1) & 0 \end{bmatrix}$$

$$p(k) = \begin{bmatrix} B_u(\phi(k))u(k) \\ -B_u(\phi(k))u(k) \\ \mathbf{1} \\ \mathbf{1} \\ \tilde{m}(k) \\ m(k-1) \end{bmatrix}$$

$$\tilde{M}(k) = \begin{bmatrix} C(\phi(k+1)) \\ -C(\phi(k+1)) \end{bmatrix}$$

$$\tilde{m}(k) = \begin{bmatrix} \bar{n} + y(k+1) \\ \bar{n} - y(k+1) \end{bmatrix}$$

$M(k-1)$ and $m(k-1)$ are defined such that $X(k) = \text{Set}(M(k-1), m(k-1))$, and $\mathbf{1}$ denotes a vector of ones of appropriate dimension. The inequality in (5) provides a description of a set in \mathbb{R}^{2n+n_d} , denoted by $\Gamma(k+1) = \text{Set}(P(k), p(k))$. Therefore, it is straightforward to conclude that

$$\hat{x} \in X(k+1) \Leftrightarrow \exists_{x \in \mathbb{R}^{n_x}, d \in \mathbb{R}^{n_d}} : [\hat{x}^T, x^T, d^T]^T \in \Gamma(k+1).$$

Hence, the set $X(k+1)$ can be obtained by projecting $\Gamma(k+1)$ onto the subspace of the first n coordinates, which, in turn, can be done resorting to the Fourier–Motzkin elimination method (see [42] and [45]). Therefore, one ends up with a description of all the admissible $x(k+1)$, which neither depends upon specific $x(k)$ nor $d(k)$.

Notice that $X(k+1)$ is, in general, a set with a large (or infinite) number of elements, rather than a singleton. Moreover, it can be obtained by the intersection of two sets, namely $\tilde{X}(k+1)$ and $Y(k+1)$, which are defined as follows:

$$\tilde{X}(k+1) = \{ \tilde{x} : \tilde{x} = A(\phi(k))x + L(\phi(k))d + B_u(\phi(k))u(k), x \in X(k), |d| \leq 1 \} \quad (6a)$$

$$Y(k) = \{ x : y(k) = C(\phi(k))x + n, |n| \leq \bar{n} \}. \quad (6b)$$

Therefore, we have that $X(k+1) = \tilde{X}(k+1) \cap Y(k+1)$. Hence, (6a) can be interpreted as a predictor that estimates where the state of the system is going to take value in the next sampling time, while (6b) can be used to update the predicted set-valued estimate of the state, based on the most recent observations. The formulation in (5) can be easily extended, in case it is convenient to compute $X(k+1)$ not only based upon $X(k)$, but also upon $X(k-1), \dots, X(k-N)$ (see [43]).

C. SVOs for LPV Dynamic Models

For plants with uncertainties, the set $X(k+1)$ is, in general, nonconvex, even if $X(k)$ is convex. Thus, it cannot be represented by a linear inequality as in (2). We are particularly interested in explicitly taking into account parametric uncertainty in the dynamic models of the systems. This type of uncertainty arises naturally from the modeling of physical

systems, such as flexible structures and vehicles moving through fluids, among others. An implementable solution to the set-valued estimation of the state of an LPV system is presented in [46]. In the suggested approach, a set-valued state estimate is provided at each time, through the vertices of a polytope, $\mathcal{P}(k)$. However, it is not guaranteed that the true state, x_{true} , is contained in $\mathcal{P}(k)$, although the minimum Euclidian distance between x_{true} and $\mathcal{P}(k)$ is guaranteed to be bounded. Implementable SVOs for LTV systems driven by exogenous disturbances were presented in [42]. One of the main advantages of this solution is that it is nonconservative. In other words, this means that, given $X(k)$ as defined in (2), the set-valued estimate of the state in the next sampling time, $X(k+1)$, contains only points that are feasible. Thus, if $x(k+1) \in X(k+1)$, then there exist $d(k)$ and $x(k)$, such that (5) is satisfied. Moreover, the method guarantees that $X(k+1)$ contains all the states that are achievable at sampling time $k+1$. Results on the extension of the work in [42] to LPV plants were presented in [43] and [44] and will be summarized next.

1) *Parametric Uncertainty in the Input Matrix:* We start by considering uncertainty in the input matrix $B_u(\phi(k))$, that is, we assume that the system can be described by

$$x(k+1) = A(\phi(k))x(k) + L(\phi(k))d(k) + B_u(\phi(k))u(k) + \sum_{j=1}^{n_\Delta} \Delta_j(k)B_j(k)u(k)$$

$$y(k) = C(\phi(k))x(k) + H(\phi(k))n(k) \quad (7)$$

where $x(0) \in X(0)$, $x(k) \in \mathbb{R}^{n_x}$, $u(k) \in U \subseteq \mathbb{R}^{n_u}$, $d(k) \in W_d \subseteq \mathbb{R}^{n_d}$, $y(k) \in \mathbb{R}^{n_y}$, $n(k) \in W_n \subseteq \mathbb{R}^{n_n}$, $\Delta(k) \in \mathbb{R}^{n_\Delta}$, $n_\Delta \in \mathbb{N}$ is the number of uncertainties, and $W_d \subseteq \mathbb{R}^{n_d}$ and $W_n \subseteq \mathbb{R}^{n_n}$ are compact convex sets. It is also assumed that

$$|\Delta_j(k)| \leq 1.$$

In this case, the uncertainty vector, $\Delta(k) = [\Delta_1(k), \dots, \Delta_{n_\Delta}(k)]^T$, represents uncertainty in the input of the plant. Define

$$F_j(k) = F_j(u(k)) = B_j(k)u(k) \quad (8)$$

for $j \in \{1, \dots, n_\Delta\}$. Then, by substituting (8) in (7), we obtain an equivalent description of the system, where each of the $\Delta_j(\cdot)$ can be seen as a bounded exogenous disturbance, acting upon the system. Hence, we recover the formulation in [42], which means that the methodology described in the previous section can be used to obtain $X(k+1)$ based on $X(k)$.

2) *Parametric Uncertainty in the Noise Matrix:* Let us consider that the noise matrix $H(\phi(k))$ is subject to parametric uncertainty, that is, the dynamic system can be described by

$$x(k+1) = A(\phi(k))x(k) + L(\phi(k))d(k) + B_u(\phi(k))u(k)$$

$$y(k) = C(\phi(k))x(k) + H(\phi(k))n(k) + \sum_{j=1}^{n_\Delta} \Delta_j(k)H_j(k)n(k) \quad (9)$$

with the same constraints as before, namely that, for each $k \in \mathbb{N}$, $|\Delta_j(k)| \leq 1$ for each $j \in \mathbb{N}$ and $n(k) \in W_n$. From (9), it follows that the output is affected by bilinear input terms of the form $\Delta_j(k)n(k)$. However, since

$|\Delta_j(k)| \leq 1$, we have that for every $k \in \mathbb{N}$, $\Delta_j(k)n(k) \in \text{co}(W_n, -W_n)$, where $\text{co}(\cdot)$ denotes the convex hull operation and $-W_n = \{n \in \mathbb{R}^{n_\Delta} : -n \in W_n\}$. To verify this, just check that for every $n(k)$, $\Delta_j(k)n(k)$ is a point in a straight line between $n(k)$ and $-n(k)$. Therefore, at the cost of some conservatism, we may consider $\Delta_j(k)n(k)$ as a new input subject to the constraint $\Delta_j(k)n(k) \in \text{co}(W_n, -W_n)$, and we may obtain $X(k+1)$ based on $X(k)$, using the methodology described in Section IV-B.

3) *Parametric Uncertainty in the Output Matrix*: Consider a dynamic system, S , described by

$$\begin{aligned} x(k+1) &= A(\phi(k))x(k) + B_u(\phi(k))u(k) + L(\phi(k))d(k) \\ y(k) &= C(\phi(k))x(k) + \sum_{j=1}^{n_\Delta} \Delta_j(k)C_j(k)x(k) + H(\phi(k))n(k) \end{aligned}$$

with the same constraints as before. In this case, the uncertainty vector, $\Delta(k)$, represents uncertainty in the output of the plant. Notice that S is equivalent to

$$\begin{aligned} S &\equiv (\bar{S}_j + H(\phi(k))\bar{n}) + \sum_{j=1}^{n_\Delta} (\Delta_j \bar{S}_j + H(\phi(k))\bar{n}) \\ \bar{S}_j &= \begin{cases} x_j(k+1) = A(\phi(k))x_j(k) + B_u(\phi(k))u(k) \\ \quad + L(\phi(k))d_i(k) \\ y_j(k) = C_j(k)x_j(k) \end{cases} \end{aligned}$$

with $j \in \{1, \dots, n_\Delta\}$, $x_j(0) = x(0)$ for all $j \in \{0, \dots, n_\Delta\}$, and $\bar{n}_i = (n_i)/(n_\Delta + 1)$.²

Since each \bar{S}_j , for $j \in \{0, \dots, n_\Delta\}$, is a linear system, and each $\Delta_j(k)$, for $j \in \{1, \dots, n_\Delta\}$ and $k \geq 0$, is an uncertain scalar, we obtain

$$\begin{aligned} S &\equiv (\bar{S}_j + H(\phi(k))\bar{n}_i) + \sum_{j=1}^{n_\Delta} (\tilde{S}_j + H(\phi(k))\bar{n}) \\ \tilde{S}_j &= \begin{cases} x_j(k+1) = A(\phi(k))x_j(k) + B_u(\phi(k))\Delta_j(k)u(k) \\ \quad + L(\phi(k))\Delta_j(k)d(k) \\ y_j(k) = C_j(k)x_j(k). \end{cases} \end{aligned} \quad (10)$$

Notice that (10) describes an LPV system with uncertain input. Nevertheless, the exogenous disturbances are now multiplied by the uncertainties $\Delta_j(k)$, and hence \tilde{S}_j depends upon $\Delta_j(k)$ and $d(k)$ in a bilinear fashion. However, this can be avoided by introducing the following relaxation. Since $|\Delta_j(k)| \leq 1$, we have that

$$\tilde{d}_j(k) = \Delta_j(k)d(k) \Rightarrow |\tilde{d}_j(k)| \leq |d(k)|. \quad (11)$$

Thus, by substituting $\Delta_j(k)d(k)$ in (10) by $\tilde{d}_j(k)$ as in (11), we obtain a description of the system that is linear in the unknown variables, at the cost of some conservatism owing to the implication in (11), that is, since $d(k)$ can impact on more than a single state, rewriting $\Delta_j(k)d(k)$ as $\tilde{d}_j(k)$ removes the coupling between $\tilde{d}_j(k)$ and $d(k)$. This method can be used to compute the set-valued estimate of the state.

²For a vector $x \in \mathbb{R}^n$, $x_i \in \mathbb{R}$ denotes the i -th entry of the vector.

4) *Parametric Uncertainty in the Dynamics*: Finally, let us consider the problem of designing SVOs for LPV plants with uncertainty in the A matrix. Let S be described by

$$S : \begin{cases} x(k+1) = A_0(\phi(k))x(k) + \sum_{j=1}^{n_\Delta} \Delta_j(k)A_j(k)x(k) \\ \quad + B_u(\phi(k))u(k) + L(\phi(k))d(k) \\ y(k) = C(\phi(k))x(k) + H(\phi(k))n(k) \end{cases} \quad (12)$$

with the aforementioned constraints. Moreover, we assume that $|\Delta_j(k)| \leq 1$. The uncertainty vector, $\Delta(k)$, represents uncertainty in the dynamics of the plant, and can appear in the modeling of several types of physical systems. Notice that the uncertainty and the state appear in (12) in a bilinear fashion. We adopt the method presented in [47] to handle this type of uncertainty. The proposed solution is to overbound the set $X(k+1)$ by a convex one, denoted by $\hat{X}(k+1)$, which is going to be described as follows. Let $v_i, i = 1, \dots, 2^{(Nn_\Delta)}$, for some positive scalar N , denote a vertex of the hypercube

$$\mathcal{C} = \{\delta \in \mathbb{R}^{Nn_\Delta} : |\delta| \leq 1\}$$

where $v_i = v_j \Leftrightarrow i = j$. Then, we denote by $\hat{X}_{v_i}(k+1)$ the set of points $x(k+1)$ that satisfy (12) with $[\Delta(k)^T, \dots, \Delta(k-N+1)^T]^T = v_i$ and with $x(k) \in \hat{X}(k), \dots, x(k-N+1) \in \hat{X}(k-N+1)$. Further define

$$\hat{X}(k+1) = \text{co}\{\hat{X}_{v_1}(k+1), \dots, \hat{X}_{v_{2^{(Nn_\Delta)}}}(k+1)\}.$$

Since $X(k+1)$ is, in general, nonconvex even if $X(k)$ is convex, we are going to use $\hat{X}(k+1)$ to overbound the set $X(k+1)$. The set $\hat{X}(k+1)$ contains $X(k+1)$, as demonstrated next.

Proposition 1 [47]: Consider a system described by (12) and assume that $X(0) \subseteq \hat{X}(0)$. Then $X(k) \subseteq \hat{X}(k)$ for all $k \in \{0, 1, 2, \dots\}$. \square

Although this approach adds some conservatism to the solution, it possesses the following valuable property.

Proposition 2 [43]: Suppose that a system described by (12) with $x(0) = X(0)$ and $u(k) = 0, \forall k$, satisfies, for sufficiently large N^*

$$\gamma_N = \max_{\substack{\Delta(k), \dots, \Delta(k+N) \\ |\Delta(m)| \leq 1, \forall m, k \geq 0}} \left\| \prod_{j=k}^{k+N} \mathcal{A}(j) \right\|_2 < 1$$

for all $N \geq N^*$, and where $\mathcal{A}(j) = A(\phi(j)) + \sum_{i=1}^{n_\Delta} A_i(j)\Delta_i(j)$. Then, $\hat{X}(k)$ cannot grow unboundedly.³ \square

Notice that, to guarantee that \hat{X} does not grow without bound, an SVO should use the N most recent estimates. In other words, the estimation of $\hat{X}(k+N)$ should take into account the fact that $x(k) \in \hat{X}(k), x(k+1) \in \hat{X}(k+1), \dots, x(k+N-1) \in \hat{X}(k+N-1)$.

D. Fault-Specific SVOs

The FDI strategy presented in this paper relies on the concept of model falsification explained in Section III. Therefore,

³Given a matrix $M \in \mathbb{R}^{m \times n}$, the operator $\|\cdot\|_2 : \mathbb{R}^{m \times n} \rightarrow \mathbb{R}_{\geq 0}$ maps M to its maximum singular value.

TABLE I
FAULT MODELING FOR THE DYNAMIC SYSTEM (13)

Type of Fault	Modeling
Changes in the Dynamics	Update A_Δ accordingly
Actuator Bias (Stuck)	$M(k) = B_u(\phi(k))$ and $m(k) = \beta$, $\beta \in \mathbb{R}$
Actuator Loss-of-Effectiveness	$M(k) = B_u(\phi(k))$ and $m(k) = (\alpha - 1)u(k)$, $\alpha \in \mathbb{R}$
Floating	$M(k) = B(\phi(k))$ and $m(k) = -u(k)$
Actuator Offset	$M(k) = B_u(\phi(k))$ and $m(k) = \beta$, $\beta \in \mathbb{R}$
Sensor Bias (Stuck)	$Q(k) = C(\phi(k))$ and $q(k) = \beta$, $\beta \in \mathbb{R}$
Sensor Loss-of-Effectiveness	$Q(k) = C(\phi(k))$ and $q(k) = (\alpha - 1)x(k)$, $\alpha \in \mathbb{R}$
Sensor Offset	$Q(k) = C(\phi(k))$ and $q(k) = \beta$, $\beta \in \mathbb{R}$

we need to design a set of SVOs that cover each plausible fault scenario. In this paper, we follow one out of two possible strategies. Depending on the kind of fault, we either:

- 1) expand the nominal model in order to deal with arbitrary but bounded changes to the parameters of the dynamic system, using the strategy presented in Section IV-C;
- 2) tune the SVO to a faulty system model.

In the latter, the uncertainty on the fault levels may be encompassed with the strategy highlighted in Section IV-C. Next, we present a system model that is versatile enough to characterize a number of different system faults.

Assume that the nominal system model is given by (1) and, for the sake of simplicity, assume that this is a single input single output (SISO) system. Then, the faulty system model is given by

$$\begin{aligned} x(k+1) &= A(\phi(k))x(k) + A_\Delta(k)x(k) + L(\phi(k))d(k) \\ &\quad + B_u(\phi(k))u(k) + M(k)m(k) \\ y(k) &= C(\phi(k))x(k) + H(\phi(k))n(k) + Q(k)q(k) \end{aligned} \quad (13)$$

where the matrices $M(k)$, $A_\Delta(k)$, $Q(k)$ and the vectors $m(k)$ and $q(k)$ can be tuned according to the specific fault under consideration, according to Table I.

E. Computational Issues

The Fourier–Motzkin algorithm, described in [45], projects polyhedral convex sets on to subspaces and leads to a set of linear inequalities, where some of them might be linearly dependent. This can be problematic, since the size of $P(k)$ and $p(k)$ [see (5)] may be increasing very fast with time. To overcome this problem, one has to eliminate the linearly dependent elements before solving for the constraints. This, in turn, can be done by solving several small linear programming problems at each sampling time. This limitation constrains the maximum number of states of the dynamic model of an SVO, and must be considered during design.

Moreover, the number of rows of $P(k)$ can also be increasing with k , as the number of vertices of the polytopes

$$\mathcal{I}(k) = \{x \in \mathbb{R}^{n_x} : x_i^{\min} \leq x_i \leq x_i^{\max}\}. \quad (14)$$

F. SVOs Versus Interval Analysis

Although the approach described in the previous subsection provides us with set-valued state estimates described by regions as in (14), it differs from the so-called interval

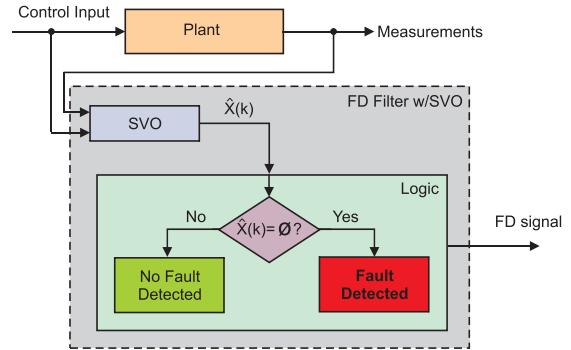


Fig. 3. FD using SVOs.

methods in the sense that the prediction and update cycles are not computed using interval analysis. Indeed, the only overbounded set is the one that comes from the intersection of $\tilde{X}(k)$ with $Y(k)$, defined by (6a) and (6b), respectively. The intermediate computations are carried using the methods described in this paper.

To further reduce the conservatism of this method, the estimate of $X(k)$ is performed not only based upon $X(k-1)$ and $Y(k)$, but also on $X(k-2)$, $X(k-3)$, \dots , $X(k-N)$, where N is a prescribed constant. As shown in Proposition 2, for sufficiently large values of the horizon, N , the set-valued estimates of the state of the system are bounded, as long as the true set containing all the possible values of the state is also bounded.

Thus, the proposed SVOs provide, in general, solutions that are less conservative than those obtained with interval analysis, although the latter method can be applied to a much larger class of plants (see [49] for further details on interval analysis).

V. FDI AND FTC USING SVOs

In this section, the applicability of the SVOs to FDI and FTC is going to be discussed. In both cases, we take advantage of the model falsification technique described in Section III to identify the model of the plant. In particular, the logic shown in Fig. 3 is used for FD, by detecting inconsistencies between the measurements obtained from the sensors and the model of the plant in nominal (nonfaulty) operation.

A. FDI Using SVOs

The FDI-SVO methodology adopted in this paper was introduced in [43] and it provides an implementation of

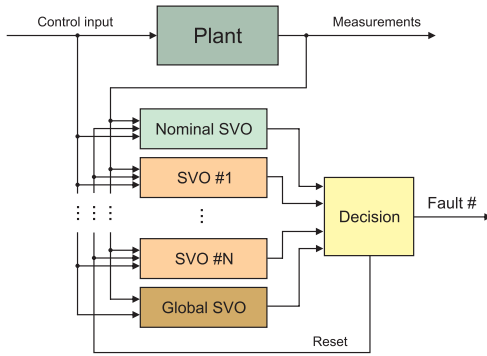


Fig. 4. FDI-SVO architecture.

the model falsification strategy described in Section III. The corresponding general architecture is shown in Fig. 4. In addition to the fault-specific SVOs, it requires two additional SVOs:

- 1) one SVO for the nonfaulty (probably uncertain and time-varying) plant—referred to as Nominal SVO;
- 2) another SVO—referred to as Global SVO—providing set-valued estimates of the state, which are valid not only for the nonfaulty plant, but also for the faulty plant. It is assumed throughout the remainder of this paper that the Global SVO always provides valid set-valued estimates. If this assumption is not met then one may not use the FDI algorithm proposed in this paper.

The Nominal SVO is used for FD only. If the state estimate of this SVO is the empty set, a fault has occurred. Hence, the fault isolation SVOs are initialized with the state estimate of the Global SVO. Since the set-valued estimate of the Global SVO is very conservative, due to being able to accommodate each possible fault, the first few iterations of the fault-specific SVOs are used mainly to reduce this conservatism.

A fault is completely isolated whenever a single fault isolation SVO has a nonempty set-valued state estimation. It should be stressed that the FD filters that are designed for specific faults, are only initialized with the set-valued state estimate of the Global SVO when they are signaled by the Nominal FD filter that a fault has occurred. Once the fault-specific SVOs are triggered, a timer is also initialized. The system returns to nominal operation when every fault-specific SVO fails or when the timer exceeds a given timeout.

The effectiveness of the proposed strategy is tied to the FDI requirements of the application at hand. In particular, if a maximum number of samples N_d is given for fault isolation, then the following assumption must be met.

Assumption 1: Given the set of system models $\mathcal{M} = \{M_0, \dots, M_{M_N}\}$ associated with the faults $\{f_0, \dots, f_{M_N}\}$ and an FDI requirement $N_d \in \mathbb{Z}$ such that $N_d > 0$, \mathcal{M} is distinguishable in N_d sampling times. \square

We have assumptions not only on the set of system model but also on the duration and separation of the faults themselves, as highlighted in the following assumptions.

Assumption 2: Given an FDI requirement $N_d \in \mathbb{Z}$ such that $N_d > 0$, if two different faults occur at times k_1 and k_2 , then $|k_1 - k_2| \geq N_d$. \square

Assumption 3: Given an FDI requirement $N_d \in \mathbb{Z}$ such that $N_d > 0$, a fault must remain active for, at least, N_d sampling times. \square

Each system model $M_i \in \mathcal{M}$ is specific of a given fault, thus if two faults occur within N_d sampling times of each other there is no model in \mathcal{M} which is able to accommodate such event, thus justifying the need for Assumption 2. If such an event is possible then one needs to add a new system model \mathcal{M} that encompasses the possibility of the two faults being simultaneously active. However, as the number of models grows, so do the computational requirements and, consequently, the slower the algorithm becomes. Since fault isolation is only guaranteed after, at least, N_d sampling times, it is an obvious requirement that the fault must remain active for N_d sampling times, as stated in Assumption 3.

If the system plant fails to meet the assumptions then the algorithm might issue an error flag. If the Global SVO does not produce the empty set-valued estimate, it may be used to repeatedly reinitialize the bank of SVOs, until the system plant returns to some behavior which is compatible with the assumptions used in the design of the FDI system, turning off the error flag. For more details, the reader is referred to [50].

B. Passive Fault-Tolerant Control

After the occurrence of a given fault, the FDI system may require several measurements before such an event is detected and isolated. Thus, in this article, we propose the use of robust controllers that, at the cost of a slight decrease in terms of performance under nonfaulty scenarios, guarantees stability of the system even under faulty environments. These controllers are designed using mixed- μ synthesis techniques that consider certain types of faults that are typically harder to detect. Hence, such robust controllers provide the FDI system with further time to determine the exact location of the fault and, then, to select a controller which is more adequate to handle the failure, as described in the following section. The synthesis of controllers that are robust against different types of uncertainties and time-variations on the dynamics of the plant has, indeed, deserved considerable attention over the last decades. The interested reader is referred to [51] and [52].

VI. WIND TURBINE MODEL

A wind turbine is composed of several parts, including: the tower, the blades, the rotor hub, the drive train, the converter, several sensors, yaw drive, controller, among others. In order to evaluate the proposed SVO-based FDI and FTC algorithms within the simulation environment described in [26], we will take advantage of the models for the rotor hub, the drive train, and the converter dynamics, therein presented. In addition, we also include the tower and flapwise blade bending models given in [53, Sec. 3].

Fig. 5 shows the connection between the different parts of the turbine considered in the dynamic model, where v_w is the wind speed, β_i denotes the i th blade pitch angle, τ_r represents the rotor torque, ω_r represents the rotor speed, τ_g represents the generator torque, ω_g represents the generator rotational speed, and P_g represents the power output. The

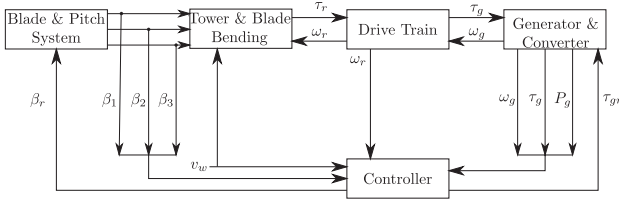


Fig. 5. Simplified wind turbine system illustrating the connections between each of its components.

controller provides pitch control and generator torque control using redundant measurements from the blades pitch ($\beta_{i_{mj}}$ for $i \in \{1, 2, 3\}$ and $j \in \{1, 2\}$), the rotor speed $\omega_{r_{mj}}$, generator speed $\omega_{g_{mj}}$, generator torque $\tau_{g_{mj}}$, and output power $P_{g_{mj}}$. These measurements are provided to the FDI algorithm along with the anemometer's readings. Each component has redundant sensors, allowing the control system to reconfigure itself when a sensor fault occurs, in order to ignore the measurements originating from the faulty sensor.

A. Aerodynamic Model

A fairly detailed description of the wind turbine aerodynamic model can be found in [1]. A very important characteristic of the aerodynamic performance of the wind turbine is its power coefficient, C_p , which is the ratio between the power delivered to the shaft P_{shaft} and the total wind power $P_{\text{wind}} = (1/2)\rho A_r v_w^3$ where $A_r = \pi R^2$ is the rotor disk area, R is the rotor radius, ρ is the atmospheric density, and v_w is the wind velocity. Using the momentum disk theory, it is possible to obtain a relation between the coefficient of power, C_p , to the coefficient of thrust, C_T as follows:

$$C_T = \frac{C_p}{1+a}$$

where $a \in \mathbb{R}$ is the axial flow interference factor, which is an aerodynamic property of the wind turbine (see [53]).

From the power delivered to the low-speed shaft, we compute the rotor torque, which is given by

$$\tau_r = \frac{P_{\text{shaft}}}{\omega_r} = \frac{1}{2} \rho \pi R^3 C_q(\lambda, \beta) v_w^2 \quad (15)$$

where ω_r is the rotor's rotational speed, $\lambda = \omega_r R / v_w$ is the tip speed ratio, β is the blade pitch,⁴ and $C_q(\lambda, \beta) = C_p(\lambda, \beta) / \lambda$ is the torque coefficient. This coefficient can be computed from experimental data or from theoretical models described throughout the literature (see [1]).

Equation (15) implicitly assumes that the pitch angle is the same for every blade. However, this is not true since each blade can control its pitch independently. Nevertheless, the rotor torque can be approximated by

$$\tau_r \approx \sum_{i=1}^3 \frac{\rho \pi R^3 C_q(\lambda, \beta_i) v_w^2}{6} \quad (16)$$

as long as the pitch angle is approximately the same for all three blades of a wind turbine (see [26]).

⁴The blade pitch is the angle between the zero lift line of the blade and the rotor disk plane.

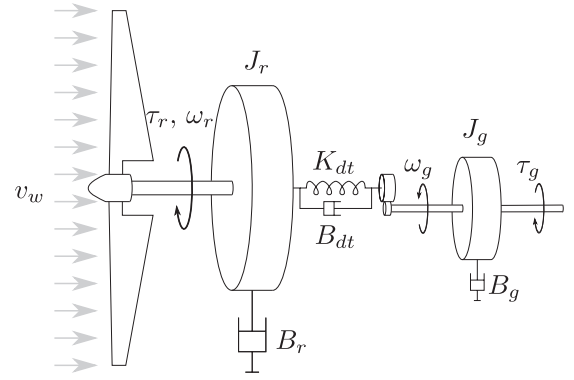


Fig. 6. Drive train system concept [55].

B. Hydraulic Pitch System Model

The blade's pitch system is usually a hydraulic mechanical system which does not instantaneously respond to reference pitch commands β_r and does not necessarily have zero static error. The transfer function of this system can be approximated by

$$\begin{bmatrix} \dot{\beta} \\ \dot{\beta}_a \end{bmatrix} = \begin{bmatrix} 0 & 1 \\ -\omega_n^2 & -2\zeta\omega_n \end{bmatrix} \begin{bmatrix} \beta \\ \beta_a \end{bmatrix} + \begin{bmatrix} 0 \\ \omega_n^2 \end{bmatrix} \beta_r \quad (17)$$

where ω_n is the nominal system's bandwidth and ζ is the nominal system's damping [26]. This simple model assumes that the pitch rate actuator is within the maximum slew rate limits.

C. Drive Train Model

The drive train is the mechanical linkage that connects the rotor to the generator. The overall system can be modeled as the connection of two masses over a shaft with finite torsion stiffness, subject to torsion damping and imperfect transmission efficiency. A gearbox converts the high rotor torque into generator speed so as to fit the requirements of a given generator. Moreover, both the rotor and the generator are subject to speed damping caused by friction. Fig. 6 shows this simplified drive train model.

The differential equations which model the dynamics of the system are given by

$$\begin{bmatrix} \dot{\omega}_r \\ \dot{\omega}_g \\ \dot{\theta}_\Delta \end{bmatrix} = \mathbf{A}_{dt} \begin{bmatrix} \omega_r \\ \omega_g \\ \theta_\Delta \end{bmatrix} + \mathbf{B}_{dt} \begin{bmatrix} \tau_r \\ \tau_g \end{bmatrix}$$

with \mathbf{A}_{dt} and \mathbf{B}_{dt} given by (as in [26])

$$\mathbf{A}_{dt} = \begin{bmatrix} -\frac{B_{dt}+B_r}{J_r} & \frac{B_{dt}}{N_g J_r} & -\frac{K_{dt}}{J_r} \\ \frac{\eta_{dt} B_{dt}}{N_g J_g} & -\frac{\eta_{dt} B_{dt} + B_g}{J_g} & \frac{\eta_{dt} K_{dt}}{N_g J_g} \\ 1 & -\frac{1}{N_g} & 0 \end{bmatrix} \quad \mathbf{B}_{dt} = \begin{bmatrix} \frac{1}{J_r} & 0 \\ 0 & \frac{1}{J_g} \\ 0 & 0 \end{bmatrix}$$

where J_r (J_g) is the rotor (generator) inertia, ω_r (ω_g) is the rotor (generator) rotational speed, B_r (B_g) is the rotor (generator) friction coefficient, K_{dt} is the shaft torsion stiffness, B_{dt} is the shaft torsion damping, η_{dt} is the shaft efficiency, θ_Δ is the torsion angle, and N_g is the gear ratio. The reader

is referred to [54] for further details regarding the drive train modeling.

D. Generator and Converter Model

The most common generator on a variable speed wind turbine is the doubly fed induction generator, whose dynamics can be modeled by the following first-order transfer function, considering that there are no faults nor saturation on the generator:

$$\frac{\tau_g}{\tau_{gr}} = \frac{\alpha_{gc}}{s + \alpha_{gc}}$$

where τ_g is the generator torque, τ_{gr} is the generator reference torque, and α_{gc} is a given parameter (see [26] or [56]). The output power, P_g , depends on the generator speed and torque, as given by $P_g = \eta_g \omega_g \tau_g$ where η_g is the efficiency of the generator. For more details on the generator model the reader is referred to [57].

E. Tower and Blade Bending

To improve the wind turbine model, we have added the dynamics associated with tower and flapwise blade bending to the benchmark model of [26], using the description that can be found in [53, Sec. 3] and the wind turbine data in [58].

This system can be modeled by the following set of linear equations:

$$\begin{bmatrix} \dot{y}_t \\ \dot{\zeta} \\ \ddot{y}_t \\ \ddot{\zeta} \end{bmatrix} = \begin{bmatrix} 0 & I_2 \\ -M^{-1}K & -M^{-1}C_{tb} \end{bmatrix} \begin{bmatrix} y_t \\ \zeta \\ \dot{y}_t \\ \dot{\zeta} \end{bmatrix} + \begin{bmatrix} 0 \\ M^{-1}Q \end{bmatrix} F_T$$

where I_n is the $n \times n$ identity matrix, 0 is an array of zeros with appropriate dimensions, $y_t \in \mathbb{R}$ is the displacement at the top of the tower, $\zeta \in \mathbb{R}$ is the flapwise deflection of the blades, $F_T \in \mathbb{R}$ is the aerodynamic force applied at the center of pressure of each blade, $r_b \in \mathbb{R}$ is the distance of the center of pressure to the turbine axis, and N_b is the number of blades. The matrices $M \in \mathbb{R}^{2 \times 2}$, $K \in \mathbb{R}^{2 \times 2}$, $C_{tb} \in \mathbb{R}^{2 \times 2}$, and $Q \in \mathbb{R}^{2 \times 1}$ are given by

$$M = \begin{bmatrix} m_t + N_b m_b & N_b m_b r_b \\ N_b m_b r_b & N_b m_b r_b^2 \end{bmatrix}, \quad K = \begin{bmatrix} K_t & 0 \\ 0 & K_b r_b^2 \end{bmatrix}$$

$$C_{tb} = \begin{bmatrix} B_t & 0 \\ 0 & B_b r_b^2 \end{bmatrix}, \quad Q = \begin{bmatrix} N_b \\ N_b r_b \end{bmatrix}$$

where $m_t, m_b \in \mathbb{R}$ is the tower/blade mass, $K_t, K_b \in \mathbb{R}$ is the tower/blade structural stiffness, and $B_t, B_b \in \mathbb{R}$ is the tower/blade damping. The oscillation of the tower and of the blades changes the effective wind speed to $v_w - \dot{y}_t - r_b \dot{\zeta}$ which, in turn, changes the aerodynamic force F_T and the aerodynamic torque τ_r [given by (16)] to

$$F_T \approx \sum_{i=1}^3 \frac{\rho \pi R^2 C_T(\lambda, \beta_i) (v_w - \dot{y}_t - r_b \dot{\zeta})^2}{6}$$

$$\tau_r \approx \sum_{i=1}^3 \frac{\rho \pi R^3 C_q(\lambda, \beta_i) (v_w - \dot{y}_t - r_b \dot{\zeta})^2}{6}$$

where $C_T(\lambda, \beta_i)$ is the coefficient of thrust.

F. Controller Regions

Wind turbines typically have four operating regions, depending on the wind conditions: Region #1—wind turbine inoperative due to low wind conditions; Region #2—the generator torque is adjusted so as to produce optimal power output; Region #3—turbine operation at rated power using aerodynamic brakes; and Region #4—the wind turbine operation is halted using hydraulic brakes to prevent structural damage due to high wind speed. In this paper, we focus on the controller design for regions #2 and #3. For more information, please see [26].

G. Faulty Scenarios

In any mechanical or electrical system, there is an infinite number of possible faulty situations. However, to keep the problem to a tractable level, we restrict our analysis to the faults listed in Table II, according to the benchmark problem in [26]. The possible faults include sensor errors, as well as changes in the dynamics of the hydraulic systems and each of these faults constitutes a threat to the turbine's operation. A level of severity is attributed to each fault, depending on the amount of damage that may result from it.

In general, sensor faults have low severity levels owing to sensor redundancy and because the controllers are typically able to reconfigure themselves to ignore any faulty sensor readings. The faults in the dynamics have higher severity levels, as they usually cause slow control actions, which may, in turn, induce permanent damage to the wind turbine. Therefore, depending on these severity levels, each fault has different FDI requirements. To fulfill the requirements in [26], the FDI algorithm described in Section VII should:

- 1) be able to detect each fault within the maximum time for detection specified in Table II;
- 2) achieve a mean time between false detections of at least 10^6 samples;
- 3) turn off a false detection after three sampling periods;
- 4) be robust to disturbances;
- 5) be able to respond rapidly to failures, by either stopping the wind turbine operation or by reconfiguring the controller structure.

In the benchmark model that is used to obtain the simulation results presented in Section VIII, we consider a sample time $T_s = 0.01$ s.

VII. FDI AND FTC OF WIND TURBINES USING SVO

In this section, we use the concepts of Section V for FDI and FTC of the wind turbine model of Section VI.

A. FDI of Wind Turbines

The first task in the implementation of the proposed FDI algorithm is to describe the wind turbine dynamics through an LPV model of the form

$$\begin{aligned} x(k+1) &= A(\phi(k))x(k) + B(\phi(k))\bar{u}(k) \\ y(k) &= C(\phi(k))x(k) + D(\phi(k))\bar{u}(k) \end{aligned} \quad (18)$$

TABLE II
FAULT SCENARIOS IMPLEMENTED IN THE WIND TURBINE BENCHMARK MODEL [26], WHERE T_s DENOTES THE SAMPLING PERIOD

No.	Fault Location	Cause	Consequence	FDI Time
1	Blade 1 Pitch Sensor 1	Electrical/mechanical	Fixed value of 5°	$10T_s$
2	Blade 2 Pitch Sensor 2	Electrical/mechanical	Decrease in gain factor by 20%	$10T_s$
3	Blade 3 Pitch Sensor 1	Electrical/mechanical	Fixed value of 10°	$10T_s$
4	Rotor sensor 1	Electrical/ mechanical	Fixed value output of 1.4 rad/s	$10T_s$
5	Rotor sensor 2	Electrical/ mechanical	Increase in gain factor by 10%	$10T_s$
5	Generator speed sensor 2	Electrical/ mechanical	Decrease in gain factor by 10%	$10T_s$
6	Blade 2 hydraulic system	Pressure drop in the hydraulic system	Modified $\omega_{n,2}$	$8T_s$
7	Blade 3 hydraulic system	Air content increase in the oil	Slow change in $\omega_{n,3}$ and ξ_3	$600T_s$
8	Generator	Offset in the internal control loop	Torque offset of 2 kN.m	$5T_s$
9	Drive train	Increased level of vibrations	Decrease of drive train efficiency by roughly 5%	-

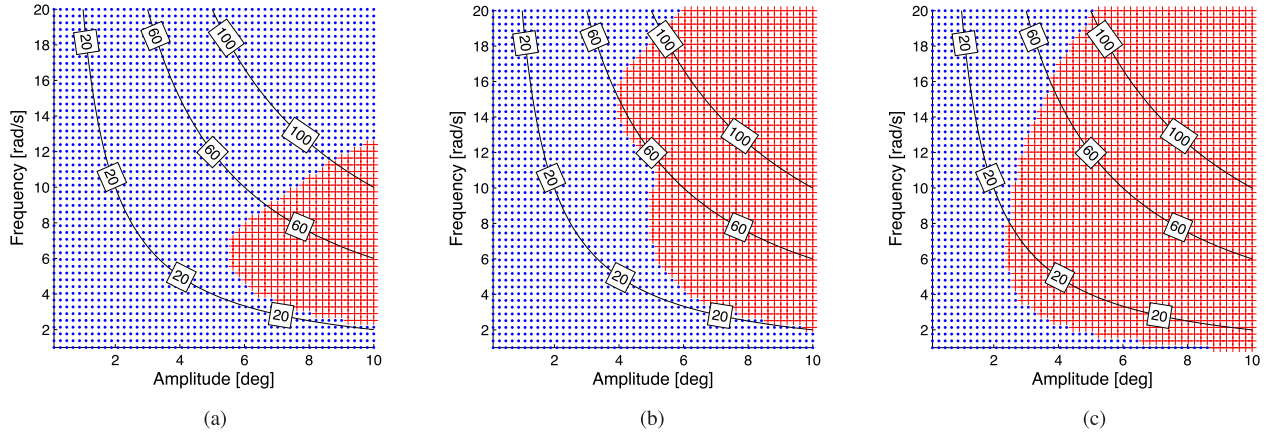


Fig. 7. FDI state machine model and the results of the distinguishability analysis. The symbols + in the grid pinpoint the parameter selection that renders the given faulty model and the nominal model distinguishable, while the symbols • pinpoint situations where the faulty model and the nominal model are indistinguishable. The curves in black depict sets of constant maximum slew rate $|A\omega|$ [$^\circ/s$]. (a) Distinguishability test for fault #2. (b) Distinguishability test for fault #6. (c) Distinguishability test for fault #7.

where $\bar{u}(k)^T = [u^T(k) d^T(k) n^T(k)]^T$, $B(\phi(k)) = [B_u(\phi(k)) L(\phi(k)) 0]$, and $D(\phi(k)) = [0 0 H(\phi(k))]$. Notice that (18) is equivalent to the framework of (1). Combining the wind turbine model described in Section VI with the LPV structure in (18) we define the state, input, and observations vectors, given by

$$\begin{aligned}
 x &= [\tau_g, \omega_r, \omega_g, \theta_\Delta, \beta_1, \beta_2, \beta_3, \dot{\beta}_1, \dot{\beta}_2, \dot{\beta}_3, x_f]^T \\
 \bar{u} &= [\tau_{gr}, \tau_r, \beta_r, n_{\tau_g}, n_{\omega_r}^{m_1}, n_{\omega_g}^{m_1}, n_{\omega_r}^{m_2}, n_{\omega_g}^{m_2}, \\
 &\quad n_{\beta_1}^{m_1}, n_{\beta_2}^{m_1}, n_{\beta_3}^{m_1}, n_{\beta_1}^{m_2}, n_{\beta_2}^{m_2}, n_{\beta_3}^{m_2}, n_{P_g^m}, u_f]^T \\
 y &= [\tau_g, \omega_{r_{m1}}, \omega_{g_{m1}}, \omega_{r_{m2}}, \omega_{g_{m2}}, P_g, \beta_{1_{m1}}, \beta_{2_{m1}}, \beta_{3_{m1}}, \\
 &\quad \beta_{1_{m2}}, \beta_{2_{m2}}, \beta_{3_{m2}}]^T
 \end{aligned}$$

respectively, where n_{τ_g} is the noise on the generator torque sensor, $n_{\omega_r}^{m_j}$ with $j = 1, 2$ is the noise on the j th rotor speed sensor, $n_{\omega_g}^{m_j}$ with $j = 1, 2$ is the noise on the j th generator speed sensor, $n_{\beta_i}^{m_j}$ with $i = 1, 2, 3$ and $j = 1, 2$ is the noise on the j th sensor of the i th blade, $n_{P_g^m}$ is the noise on the power sensor, x_f and u_f are the state and the input of a high pass filter, respectively, with transfer function

$$H(s) = \frac{\omega_f s}{s + \omega_f}$$

where $\omega_f \in \mathbb{R}$. This high pass filter is applied to the measurements of the first rotor sensor, providing the SVOs

with the information that the measurement noise has zero expected value. This approach aids the detection of fault #4 (see Table II).

According to these definitions, the continuous-time state-space matrices $A(\phi(t))$, $B(\phi(t))$, $C(\phi(t))$, and $D(\phi(t))$ are given by (20) shown at the top of the next page. It is clear from (20) that the scheduling variable is $\phi(t) = \omega_g(t)$.

To conclude the implementation of the nominal SVO (see Fig. 8), it is necessary to define the vectors $b^+(k)$ and $b^-(k)$, which are upper and lower bounds on $\bar{u}(k)$, respectively, that is, $b^-(k) \leq \bar{u}(k) \leq b^+(k)$. Since the sensor noise is considered to be Gaussian white noise, the noise vector bounds on the sensor s can be characterized through its standard deviation σ_s . The vectors $b^+(k)$ and $b^-(k)$ are given by

$$\begin{aligned}
 b^+(k) &= [\tau_g(k), \tau_r^+(k), \beta_r(k), k_\sigma \sigma_{\tau_g}, k_\sigma \sigma_{\omega_r}, k_\sigma \sigma_{\omega_g}, \\
 &\quad k_\sigma \sigma_{\omega_r}, k_\sigma \sigma_{\omega_g}, k_\sigma \sigma_{\beta} \mathbf{1}, k_\sigma \sigma_{P_g}(k)]^T \\
 b^-(k) &= [\tau_g(k), \tau_r^-(k), \beta_r(k), -k_\sigma \sigma_{\tau_g}, -k_\sigma \sigma_{\omega_r}, -k_\sigma \sigma_{\omega_g}, \\
 &\quad -k_\sigma \sigma_{\omega_r}, -k_\sigma \sigma_{\omega_g}, -k_\sigma \sigma_{\beta} \mathbf{1}, -k_\sigma \sigma_{P_g}(k)]^T \quad (19)
 \end{aligned}$$

where σ_s is the standard deviation of the sensor s , and τ_r^+ and τ_r^- are suitable upper and lower bounds to the aerodynamic torque τ_r . In the benchmark model used for the simulations, it is assumed that the sensor noise is Gaussian and, because the SVO-based strategy revolves around the fact that the noise/disturbances are bounded, we have to accept that the

where a , w , and b , are the amplitude, the frequency, and the bias of the sinusoid, respectively. This excitation is applied to the reference input of the blades' pitch angles when they are at rest (controller region #2) in order to facilitate the identification of changes in the dynamics. In this section, we show that the nominal system and the faulty systems generated by faults #2, #6, and #7 are not distinguishable when the blades remain at rest. In fact, the distinguishability analysis presented here shows that these systems are not distinguishable for a vast range of frequencies and amplitudes of the input signal. The controller for region #3 already has nonzero reference pitch, unlike the controller for region #2, and it operates at higher wind speeds, which should provide higher input excitation, thus we restrict our analysis to the distinguishability between the nominal and faulty systems during the operation in region #2.

To keep the analysis to a tractable level, we choose the parameters A and w using the strategy in Section III-A, where the key idea is to guarantee that the nominal and the faulty systems are distinguishable from each other (see [35]), and we assigned $b = 2^\circ$ and $N_d = 40T_s$, meaning that the distinguishability will be tested for a fixed horizon of 100 sampling periods. It should be pointed out that N_d is a very important parameter in any distinguishability test. As N_d increases, we also increase the chance that any two given models are distinguishable since we are less likely to find matching outputs, for a given set of possible inputs, over longer periods of time. For the particular wind turbine considered, we obtain the results shown in Fig. 7, by assuming $b = 7^\circ$ to avoid the saturation of the blades, and where the red dots indicate that the systems are distinguishable for the corresponding values of A and w . Therefore, if the reference signal for the blades' pitch angles is described by

$$\eta_r(t) = 8 \sin(6t) + 7 \quad (21)$$

we guarantee the distinguishability between the nominal model and the model associated to fault #2 [Fig. 7(a)], the model associated to fault #6 [Fig. 7(b)], and the model associated with fault #7 [Fig. 7(c)]. We have chosen solely these models for the distinguishability analysis, because they were the ones that proved to be the most challenging from a FDI perspective.

The reader should be aware that the input excitation (21) is not feasible whenever the input signal exceeds the maximum slew rate limitations of the pitch system. If this is the case, then the power of the input (21) must be reduced to feasible values at the expense of FDI performance. For example, in our setup, the input signal (21) has a slew rate of $48^\circ/\text{s}$. Attempts were made to reduce the slew rate down to $15^\circ/\text{s}$, but the isolation performance of faults number #2 and #6 was severely affected by this change, taking up to 30 s to isolate either fault.

Other drawbacks of the input injection signal include the additional structural stress to the wind turbine and the sub-optimal energy extraction. Therefore, a compromise between FD, structural integrity and energy extraction must be made and, as a result, the wind turbine operator, may choose to use this input injection signal more sparingly. For the purposes of illustrating the capabilities of the FDI strategy that we

propose, we have opted for improved FDI performance, at the cost of additional structural stress and reduced output power.

C. FTC of Wind Turbines

Under faulty scenarios, the use of controllers designed for the nominal operation of the plant can lead to severe performance deterioration and, ultimately, to damage of the wind turbine [26]. The FTC-SVO architecture that we employ is depicted in Fig. 8. The Decision-block is responsible for selecting the appropriate controller, based upon the set-valued estimates provided by the bank of SVOs. Each controller is designed so that robust-stability is guaranteed while a given fault is not detected and isolated. The FTC-SVO method uses a mixed solution, between an active FDI algorithm and a passive FTC as follows.

1) *Active*: The FDI system applies input excitation to the plant, whenever the measured signals hinder the distinguishability of the faults—see Section III-A. If the system is operating normally, the Nominal SVO provides nonempty set-valued state estimates for the plant, and thus the Nominal Controller is connected to the loop. This controller must also be able to accommodate a fault, should it occur, until the FDI algorithm (see Section V-A) detects and isolates this fault. After that, if fault # i is isolated, then controller # i will be connected to the loop, substituting the nominal one. The controller is reconfigured according to the details provided in Table III.

2) *Passive*: The controller synthesized for the nominal system is also robust to mild variations on the dynamics of the plant, so that faults can be accommodated while the FDI subsystem is not able to reconfigure the controller. Such controller accounts for parametric uncertainties and process disturbances, allowing the operation of the wind turbine under low severity faulty scenarios. The robust controllers are mostly important during the operation of the wind turbine under the faults number 6–9, as can be seen in Table III.

D. Robust Controller Design

The synthesis of controllers that are robust against different types of uncertainties and time-variations on the dynamics of the plant has deserved considerable attention over the last decades. The interested reader is referred to [51] and [52]. Among the many alternatives in the literature, the technique adopted in this paper is referred to as mixed- μ synthesis. A mixed- μ controller is an approximation of the optimal controller in the \mathcal{L}_2 -induced norm sense, from the exogenous inputs to the performance outputs. Despite the suboptimality of the solution, these controllers are capable of handling different types of uncertainties, namely complex and parametric uncertainties, resorting to the so-called D, G-K iterations (see [59] and [60], and references therein).

The wind turbine model described in Section VII-A was used to the synthesis of the mixed- μ controller, with the additional requirement that the closed-loop system remains stable not only under nominal operation, but also in the presence of faults #6 or #7. Therefore, the dynamics of the blades can be described by (17), where $\omega_n \in [3.42, 11.11]$ rad/s and

TABLE III
SCHEDULED ACTIONS TRIGGERED DURING FAULT IDENTIFICATION EVENTS

No.	Fault Location	Action
1	Blade 1 Pitch Sensor 1	Switch to Blade 1 Pitch Sensor 2
2	Blade 2 Pitch Sensor 2	Switch to Blade 2 Pitch Sensor 1
3	Blade 3 Pitch Sensor 1	Switch to Blade 3 Pitch Sensor 2
4	Rotor sensor 1	Switch to Rotor sensor 2
5	Rotor sensor 2	Switch to Rotor sensor 1
5	Generator speed sensor 2	Switch to Generator speed sensor 1
6	Blade 2 hydraulic system	Stop turbine operation
7	Blade 3 hydraulic system	Do nothing (fault handled by robust controller)
8	Generator	Do nothing (fault handled by robust controller)
9	Drive Train	Do nothing (fault handled by robust controller)

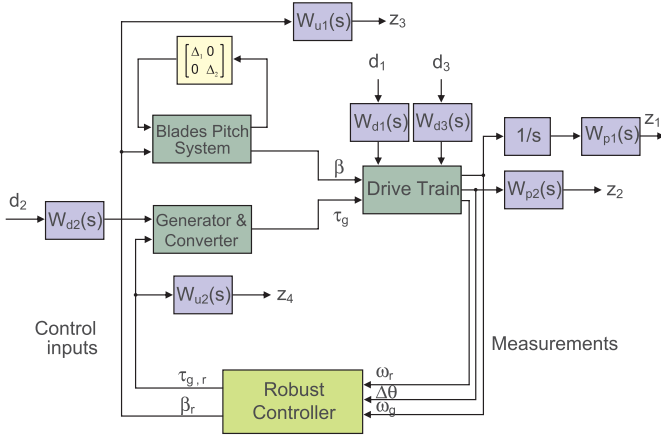


Fig. 9. Block diagram for robust controller synthesis of the wind turbine model.

$\zeta \in [0.25, 0.9]$. In this methodology, the selection of the dynamic weights is key to ensure proper disturbance rejection at the desired frequencies, as well as to avoid high-frequency command signals to be sent to the control inputs. Thus, the approach adopted in this paper is fully described in [61], and consists in optimizing a given performance criterion. In this particular case, the design diagram used is shown in Fig. 9, and the weights were selected as follows:

$$\begin{aligned}
 W_{d1} &= \frac{1}{s+1}, & W_{d2} &= 1 \times 10^3 \frac{1}{s+1} \\
 W_{d3} &= \frac{3}{s+30}, & W_{u1} &= 0.6 \frac{s+0.1}{s+100} \\
 W_{u2} &= 1 \times 10^{-3} \frac{s+10}{s+100}, & W_{p1} &= A_{p1} \frac{1}{s+0.1} \\
 W_{p2} &= A_{p2}, & W_{p3} &= \frac{A_{p3}}{s+1} \\
 W_{p4} &= A_{p4}, & W_{p5} &= A_{p5}.
 \end{aligned}$$

By maximizing the values of $A_{p1}, A_{p2}, \dots, A_{p5}$, while guaranteeing a value of μ smaller than one, we obtain: $A_{p1} = 0.009$, $A_{p2} = 0.008$, $A_{p3} = 1$, $A_{p4} = 1 \times 10^{-4}$, and $A_{p5} = 1 \times 10^{-4}$.

The mixed- μ design method briefly described above assumes that the linearized model of the wind turbine is an accurate description of the corresponding dynamics. Nevertheless, a linearization is typically performed around a trimming point. This trimming point, in turn, depends solely on the wind speed, since nominal values of all state variables can be

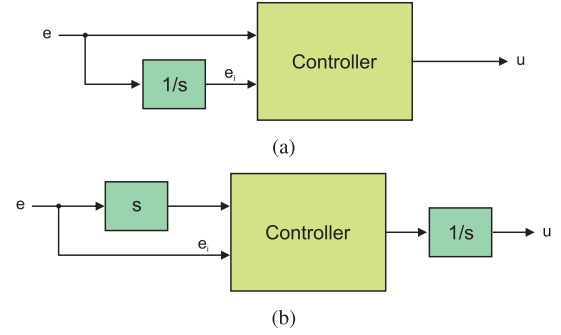


Fig. 10. D-Methodology. (a) Controller with integral states. (b) Controller with integrator at the output.

obtained as functions of v_w . Hence, as soon as the linearized model, for a particular value of v_w , no longer describes the dynamics of the wind turbine, a controller designed for the current value of the wind speed should be connected to the loop. Although a detailed discussion on this topic is out of the scope of this paper, it is worthwhile to mention that this scheduling between controllers has been widely analyzed in the literature of LPV control, and a broad class of systems, ranging from aircrafts to chemical processes, are nowadays equipped with this type of controllers. For further details, the reader is referred to [62].

In this paper, three different regions are considered for the wind speed, as they lead to linearized models of the wind turbine that accurately cover the typical behaviors of this system (see [63]). Indeed, the first model was obtained by linearizing the model of the dynamics of the wind turbine around $\bar{v}_w^1 = 13$ m/s, while the second one considered $\bar{v}_w^2 = 15$ m/s, and the third one assumed $\bar{v}_w = 17$ m/s.

With the estimated wind speed, the appropriate mixed- μ controller is connected to the loop. For the sake of simplicity, the controller is selected by the trimming wind speed which is closest (in the Euclidean norm sense) to the estimated wind speed. Thus, the following regions are obtained: $\Omega_1 = [0, 14]$ m/s, $\Omega_2 = [14, 16]$ m/s, and $\Omega_3 = [16, v_w^{\max}]$ m/s where v_w^{\max} is such that the wind turbine is shut down if the estimated wind speed exceeds that value.

Each robust controller was implemented using the so-called D-Methodology (see [64]) which will be briefly described in the sequel. The main idea from this approach stems from the fact that the transfer functions of the block diagrams in Fig. 10 are the same. Therefore, from the point of view of the

linearized system, the use of either the controller in Fig. 10(a) or the one in Fig. 10(b) is irrelevant.

However, having an integrator at the output of the controller has several advantages in terms of implementation in a nonlinear system. The methodology shown in Fig. 10(a) ensures that the linearization of the nonlinear closed-loop system about the equilibrium points preserve the same internal structure as well as input–output properties of the corresponding linear closed loop designs. Moreover, the use of integral action guarantees zero steady-state error for the selected outputs and, since it is placed at the plant input, the need to feedforward trimming values for the actuation signals and outputs not required to track references is eliminated. Moreover, the use of an integrator at the output of the controller also facilitates the implementation of antiwindup techniques, that accelerate the response of the system when some of the actuators are saturated.

Finally, in the gain-scheduling approach described in the previous section, one can also experience large transients due to the switching of the controllers if an integrator is not used. Hence, even if the switching between the controllers generates discontinuous signals, the integrator smooths out the command signals sent to the plant.

As a technical comment, the derivatives shown in Fig. 10(b), owing to implementation constraints imposed by causality, should be in series with a low-pass filter.

VIII. SIMULATION RESULTS

In this section, we present some simulation results on FTC/FDI of wind turbines using the benchmark model presented in [26], using a sampling period of $T_s = 0.01$ s. The simulations were split into three different cases.

- 1) Comparison between the robust controller and the PID controller described in [26], under the influence of different faults, using neither the FDI apparatus nor the controller reconfiguration strategy.
- 2) Monte Carlo simulations of the FDI system using the robust controller.
- 3) Simulations of the whole system, mainly to test the active FTC strategy outlined in Section V.

The PID controller was tuned to track the nominal speed of the rotor (see [26]) and the mixed- μ controller was designed according to the details given in the previous section. Neither was designed taking into consideration the effects of tower and blade vibration. Therefore, by running the simulations with and without the vibrations, we are able to assess the performance of both controllers to plant uncertainties. We ran a total of ten Monte Carlo simulations for each controller and for each operating scenario—nominal operation and operation under the influence of the faults 6 and 7—using randomly generated wind sequences, within the modified wind turbine benchmark model described in Section VI (Fig. 11 shows six examples of wind sequences). For more information on the modeling of the windspeed, the reader is referred to [65]. For the batch of Monte Carlo simulations without tower/blade vibrations, we obtained the results listed in Table IV, while for the batch of simulations that include the tower/blade

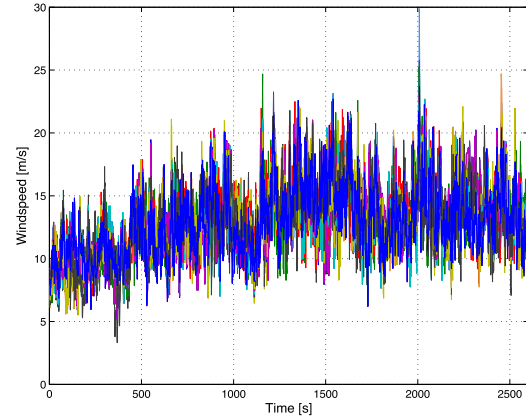


Fig. 11. Superimposed wind sequences that were used in the Monte Carlo experiments.

TABLE IV
RESULTS FROM THE MONTE CARLO SIMULATIONS OF THE ROBUST CONTROLLER WITHOUT THE EFFECTS OF TOWER AND BLADE VIBRATIONS

		Standard deviation of the output power σ_{P_g} [kW]	Standard deviation of the generator speed σ_{ω_g} [rad/s]
Nominal	PID	43	3.8
	mixed- μ	30	5.4
Fault # 6	PID	58	4.3
	mixed- μ	30	5.4
Fault # 7	PID	62	4.5
	mixed- μ	30	5.5

TABLE V
RESULTS FROM THE MONTE CARLO SIMULATIONS OF THE ROBUST CONTROLLER UNDER THE EFFECT OF TOWER AND BLADE VIBRATIONS

		Standard deviation of the output power σ_{P_g} [kW]	Standard deviation of the generator speed σ_{ω_g} [rad/s]
Nominal	PID	214	4.2
	mixed- μ	89	5.4
Fault # 6	PID	213	3.8
	mixed- μ	79	5.1
Fault # 7	PID	214	4.3
	mixed- μ	92	5.5

vibrations, the results are listed in Table V. Comparing the results from these two sets of simulations, it is possible to verify that the performance of the PID controller is more

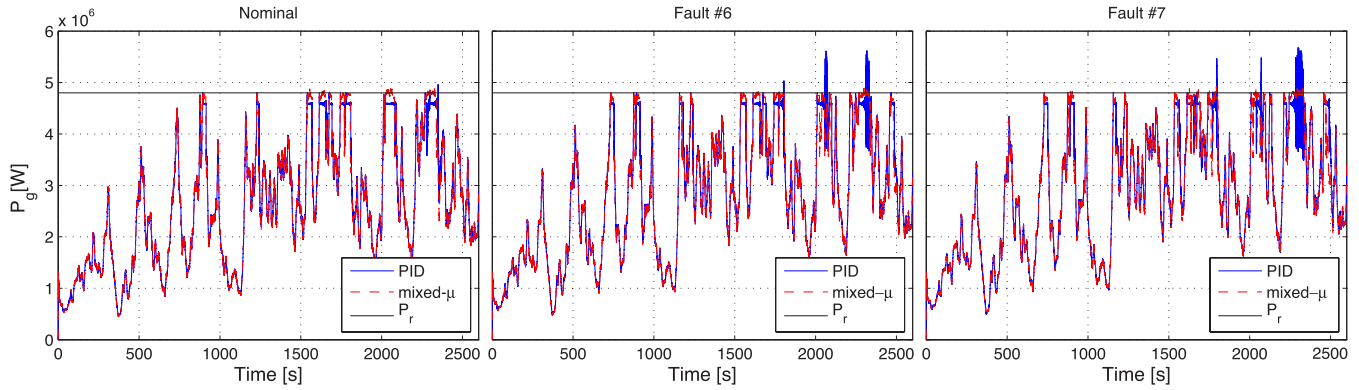


Fig. 12. Comparison of the PID and the mixed- μ controllers in terms of the output power P_g , under the influence of blade and tower vibrations, and for three different operating conditions.

TABLE VI
FD SIMULATIONS RESULTS

Fault no.	Median Detection Time [s]	Max. Detection Time [s]	Median Isolation Time [s]	Max. Isolation Time [s]	Laouti et. al [67]	Zhang et. al [68]	Ozdemir et. al [69]
1	0.01	0.01	0.01	0.02	0.01	-	0.03
2	0.01	0.05	0.045	3.13	0.66	-	8.194
3	0.01	0.01	0.01	0.01	0.01	0.5	0.03
4	0.06	0.06	0.06	0.11	0.01	0.35	0.124
5	0.01	0.01	0.01	0.01	0.66	0.01	1.874
6	0.18	0.20	0.27	0.32	-	-	50.50
7	7.12	8.89	7.125	8.9	-	10	15.73
8	0.01	0.01	0.01	0.04	0.01	0.01	0.01

deteriorated than that of the mixed- μ controller, as the tracking error of the nominal output power ($P_r = 4.8$ MW) substantially increases, unlike what is observed using the mixed- μ controller. In Fig. 12, we show the output power P_g for a time span of 2600 s, where the controller changes from the controller of region #2 to the controller of region #3, when $\omega_g \geq 165$ rad/s or $P_g \geq P_r = 4.8$ MW. On the other hand, the selected controller changes from the controller of region #3 to the controller of region #2 if $\omega_g \leq 147$ rad/s. This is the same logic that is described in [26]. Since the robust controller is only used in region #3, one can only notice the differences between the two controllers when the reference output power is being tracked. In this situation, it can be seen that the robust controller tracks the reference without bias, unlike the PID controller, and with much smaller variation. Moreover, we added a low pass filter with a bandwidth of 20 rad/s at the output of both controllers and we also verify that the performance of the PID controller is degraded, unlike the performance of the robust controller, meaning that the PID is injecting high frequency signals into the system plant.

The second batch of simulations includes the application of the SVO strategy described in Section VII (using $N = 10$ for the nominal SVO) to the closed loop system resulting from the interconnection between the wind turbine system and the FTC described in Section VII-D instead of the standard PID controller. The computation of the bank of SVOs is highly time consuming, taking roughly 45 s to complete a single second in the simulation (using an workstation with Dual Xeon

processors at 2.4 GHz with six cores each and 24 GB of high-speed RAM). Therefore, we restricted the simulation to a span of 15 s, where the fault occurs 5 s after the beginning of the run. It should be noticed, however, that the banks of SVOs can take advantage of recent advances in low-cost multicore processors, as the structure of the proposed architecture is highly parallelizable.

The simulation results for 40 simulation runs of each of the faults are presented in Table VI. For the most part, the obtained results comply with the FDI requirements of [26]. The exceptions are the detection of faults 6 and 7 and the isolation of fault 2. Nevertheless, comparing the obtained results with those from the FDI strategies presented in [66], [67], and [68] (for the same benchmark model), we verify that the performance in the detection of sensor faults is similar to other strategies and the performance in the isolation of faults 6 and 7 surpasses them. The main exception is fault number 4, whose detection and isolation times are surpassed by the strategy in [66].

Plugging the proposed FDI algorithm into the closed loop simulation using the architecture described in Section V, we obtain a sequence of active controllers which is represented in Fig. 13 and the corresponding controller architecture is applied (see Table III). In this figure, it is possible to see that faults are identified correctly, since the algorithm chooses the appropriate controller once the fault is identified. However, there exists a lag in the recovery from a fault. The algorithm takes up to 100 s to return to nominal operation once the fault

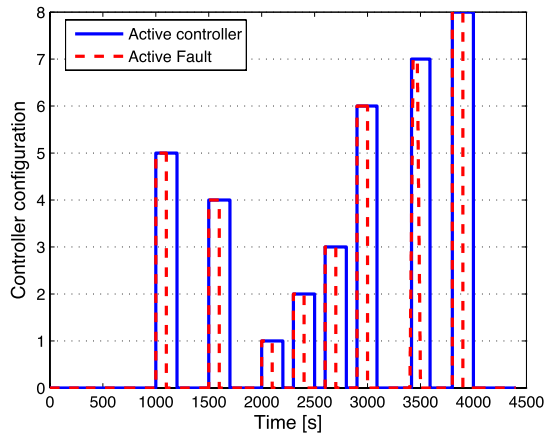


Fig. 13. Active controller configuration for a particular benchmark simulation run. The value 0 corresponds to the default controller configuration. The controller configurations $k \in \{1, \dots, 8\}$ correspond to each one of the actions listed in Table III.

has vanished. This is enforced by design, in an attempt to avoid false recoveries, i.e., situations where the controller returns to nominal operation but the fault is still active. For more details on the implementation of the proposed FDI strategy, the reader is invited to check [69].

IX. CONCLUSION

This paper described FDI and FTC methodologies, applicable to LPV systems that take advantage of recent advances in the SVOs theory to invalidate dynamic models. In particular, we focus on the applicability of the method to wind turbines, where such methodologies can have a significant impact. Contrary to residual-based approaches, the suggested method does not need the computation of decision thresholds, which are highly dependent on the exogenous disturbances, measurement noise, and model uncertainty. Some of the computational issues that arise in the implementation of such methods are also briefly discussed. In terms of FTC, a mixed active-passive approach was adopted. In particular, robust controllers were used to accommodate faults during the period the FDI system is trying to isolate them. Once a fault is isolated, the controller is reconfigured so as to minimize the impact on the closed-loop plant. Monte Carlo simulations were performed on a faulty wind turbine, showing that only a few measurements are necessary, in general, to detect and isolate faults.

However, the effectiveness of the proposed strategy is dependent on the availability of large computational resources. Conservative approximations of the set-valued estimates may be used to speed up the process at the cost of FDI performance. A quantitative analysis on the implications of such approximations is the subject of active research, and should be part of our future work.

REFERENCES

- [1] T. Burton, D. Sharpe, N. Jenkins, and E. Bossanyi, *Wind Energy Handbook*. New York, NY, USA: Wiley, 2001.
- [2] Z. Hameed, Y. Hong, Y. Cho, S. Ahn, and C. Song, "Condition monitoring and fault detection of wind turbines and related algorithms: A review," *Renew. Sustain. Energy Rev.*, vol. 13, no. 1, pp. 1–39, 2009.

- [3] A. Willsky, "A survey of design methods for failure detection in dynamic systems," *Automatica*, vol. 12, no. 6, pp. 601–611, 1976.
- [4] M. Blanke, M. Staroswiecki, and N. Wu, "Concepts and methods in fault-tolerant control," in *Proc. Amer. Control Conf.*, Arlington, VA, USA, Jun. 2001, pp. 2606–2620.
- [5] R. Patton and J. Chen, "Observer-based fault detection and isolation: Robustness and applications," *Control Eng. Pract.*, vol. 5, no. 5, pp. 671–682, 1997.
- [6] P. Frank and X. Ding, "Survey of robust residual generation and evaluation methods in observer-based fault detection systems," *J. Process Control*, vol. 7, no. 6, pp. 403–424, 1997.
- [7] A. M. Esteban, "Aircraft applications of fault detection and isolation techniques," Ph.D. dissertation, Dept. Aerosp. Eng. Mech., Univ. Minnesota, Minneapolis, MN, USA, 2004.
- [8] E. G. Collins, Jr. and S. Tinglun, "Robust l_1 estimation using the Popov–Tsytkin multiplier with application to robust fault detection," *Int. J. Control*, vol. 74, no. 3, pp. 303–313, 2001.
- [9] S. Longhi and A. Moteriu, "Fault detection for linear periodic systems using a geometric approach," *IEEE Trans. Autom. Control*, vol. 54, no. 7, pp. 1637–1643, Jul. 2009.
- [10] P. Frank and X. Ding, "Frequency domain approach to optimally robust residual generation," *Automatica*, vol. 30, no. 5, pp. 789–804, 1994.
- [11] N. Meskin and K. Khorasani, "Fault detection and isolation of discrete-time Markovian jump linear systems with application to a network of multi-agent systems having imperfect communication channels," *Automatica*, vol. 45, no. 9, pp. 2032–2040, 2009.
- [12] D. Wang, W. Wang, and P. Shi, "Robust fault detection for switched linear systems with state delays," *IEEE Trans. Syst., Man, Cybern. B, Cybern.*, vol. 39, no. 3, pp. 800–805, Jun. 2009.
- [13] S. Narasimhan, P. Vachhani, and R. Rengaswamy, "New nonlinear residual feedback observer for fault diagnosis in nonlinear systems," *Automatica*, vol. 44, no. 9, pp. 2222–2229, 2008.
- [14] M. A. Massoumnia, "A geometric approach to the synthesis of failure detection filters," *IEEE Trans. Autom. Control*, vol. 31, no. 9, pp. 839–846, Sep. 1986.
- [15] J. Bokor and G. Balas, "Detection filter design for LPV systems—A geometric approach," *Automatica*, vol. 40, no. 3, pp. 511–518, 2004.
- [16] A. Edelmayer, J. Bokor, and L. Keviczky, "An \mathcal{H}_∞ approach to robust detection of failures in dynamical systems," in *Proc. 33rd Conf. Decision Control*, vol. 3. Lake Buena Vista, FL, USA, Dec. 1994, pp. 3037–3039.
- [17] H. Niemann and J. Stoustrup, "Fault diagnosis for non-minimum phase systems using H_∞ optimization," in *Proc. Amer. Control Conf.*, Arlington, VA, USA, Jun. 2001, pp. 4432–4436.
- [18] A. Marcos, S. Ganguli, and G. Balas, "An application of \mathcal{H}_∞ fault detection and isolation to a transport aircraft," *Control Eng. Pract.*, vol. 13, no. 1, pp. 105–119, 2005.
- [19] R. Mangoubi, B. Appleby, G. Verghese, and W. V. Velde, "A robust failure detection and isolation algorithm," in *Proc. 34th Conf. Decision Control*, vol. 3. New Orleans, LA, USA, 1995, pp. 2377–2382.
- [20] A. Savkin and I. Petersen, "Model validation for robust control of uncertain systems with an integral quadratic constraint," *Automatica*, vol. 32, no. 4, pp. 603–606, 1996.
- [21] C. Combastel and S. Raka, "A set-membership fault detection test with guaranteed robustness to parametric uncertainties in continuous time linear dynamical systems," in *Proc. Fault Detection, Supervision Safety Tech. Process.*, 2009, pp. 1192–1197.
- [22] A. Ingimundarson, J. Bravo, V. Puig, T. Alamo, and P. Guerra, "Robust fault detection using zonotope-based set-membership consistency test," *Int. J. Adaptive Control Signal Process.*, vol. 23, no. 4, pp. 311–330, 2009.
- [23] J. Stoustrup and H. Niemann, "Active fault diagnosis by controller modification," *Int. J. Syst. Sci.*, vol. 41, no. 8, pp. 925–936, 2010.
- [24] N. Poulsen and H. Niemann (2008, Dec.). Active fault diagnosis based on stochastic tests. *Int. J. Appl. Math. Comput. Sci.* [Online]. 18(4), pp. 487–496. Available: <http://dx.doi.org/10.2478/v10006-008-0043-6>
- [25] S. M. Tabatabaeipour, "Active fault detection and isolation of discrete-time linear time-varying systems: A set-membership approach," *Int. J. Syst. Sci.*, to be published, doi:10.1080/00207721.2013.843213.
- [26] P. F. Odgaard, J. Stoustrup, and M. Kinnaert, "Fault tolerant control of wind turbines—A benchmark model," in *Proc. 7th Symp. Fault Detection, Supervision Safety Tech. Process.*, 2009.
- [27] P. Casau, P. Rosa, S. Tabatabaeipour, and C. Silvestre, "Fault detection and isolation and fault tolerant control of wind turbines using set-valued observers," in *Proc. 8th Symp. Fault Detection, Supervision Safety Tech. Process.*, 2011.

- [28] K. Poolla, P. Khargonekar, A. Tikku, J. Krause, and K. Nagpal, "A time-domain approach to model validation," *IEEE Trans. Autom. Control*, vol. 39, no. 5, pp. 951–959, May 1994.
- [29] F. Bianchi and R. Sánchez-Peña, "Robust identification/invalidation in an LPV framework," *Int. J. Robust Nonlinear Control*, vol. 20, no. 3, pp. 301–312, 2010.
- [30] R. Nikoukhah, S. L. Campbell, K. G. Horton, and F. Delebecque, "Auxiliary signal design for robust multimodel identification," *IEEE Trans. Autom. Control*, vol. 47, no. 1, pp. 158–164, Jan. 2002.
- [31] R. Nikoukhah and S. L. Campbell, "Auxiliary signal design for active failure detection in uncertain linear systems with a priori information," *Automatica*, vol. 42, no. 2, pp. 219–228, 2006.
- [32] H. H. Niemann and N. K. Poulsen, "Active fault diagnosis in closed-loop systems," in *Proc. 16th IFAC World Congr.*, 2005.
- [33] H. H. Niemann, "A setup for active fault diagnosis," *IEEE Trans. Autom. Control*, vol. 51, no. 9, pp. 1572–1578, Sep. 2006.
- [34] S. Tabatabaeipour, "Fault diagnosis and fault-tolerant control of hybrid systems," Ph.D. dissertation, Dept. Electron. Syst., Aalborg Univ., Aalborg, Denmark, 2010.
- [35] P. Rosa and C. Silvestre, "On the distinguishability of discrete linear time-invariant dynamic systems," in *Proc. 50th IEEE Conf. Decision Control*, Dec. 2011, pp. 3356–3361.
- [36] H. Witsenhausen, "Sets of possible states of linear systems given perturbed observations," *IEEE Trans. Autom. Control*, vol. 13, no. 5, pp. 556–558, Oct. 1968.
- [37] F. Schweppe, "Recursive state estimation: Unknown but bounded errors and system inputs," *IEEE Trans. Autom. Control*, vol. 13, no. 1, pp. 22–28, Feb. 1968.
- [38] F. Schweppe, *Uncertain Dynamic Systems*. Englewood Cliffs, NJ, USA: Prentice-Hall, 1973.
- [39] M. Milanese and A. Vicino, "Optimal estimation theory for dynamic systems with set membership uncertainty: An overview," *Automatica*, vol. 27, no. 6, pp. 997–1009, 1991.
- [40] F. Yang and L. Yongmin, "Set-membership filtering for discrete-time systems with nonlinear equality constraints," *IEEE Trans. Autom. Control*, vol. 54, no. 10, pp. 2480–2486, Oct. 2009.
- [41] M. Baglietto, G. Battistelli, and L. Scardovi, "Active mode observation of switching systems based on set-valued estimation of the continuous state," *Int. J. Robust Nonlinear Control*, vol. 19, no. 14, pp. 1521–1540, 2009.
- [42] J. Shamma and K.-Y. Tu, "Set-valued observers and optimal disturbance rejection," *IEEE Trans. Autom. Control*, vol. 44, no. 2, pp. 253–264, Feb. 1999.
- [43] P. Rosa, C. Silvestre, J. Shamma, and M. Athans, "Fault detection and isolation of LTV systems using set-valued observers," in *Proc. 49th IEEE CDC*, Dec. 2010, pp. 768–773.
- [44] P. Rosa, C. Silvestre, and M. Athans, "Model falsification of LPV systems using set-valued observers," in *Proc. 18th IFAC World Congr.*, Aug./Sep. 2011.
- [45] S. Keerthi and E. Gilbert, "Computation of minimum-time feedback control laws for discrete-time systems with state-control constraints," *IEEE Trans. Autom. Control*, vol. 32, no. 5, pp. 432–435, May 1987.
- [46] H. Lin, G. Zhai, and P. J. Antsaklis, "Set-valued observer design for a class of uncertain linear systems with persistent disturbance and measurement noise," *Int. J. Control*, vol. 76, no. 16, pp. 1644–1653, 2003.
- [47] P. Rosa, "Multiple-model adaptive control of uncertain LPV systems," Ph.D. dissertation, Dept. Elect. Comput. Eng., Inst. Superior Técnico, Lisbon, Portugal, 2011.
- [48] F. Blanchini and S. Miani, *Set-Theoretic Methods in Control*. Basel, Switzerland: Birkhäuser Basel, 2007.
- [49] L. Jaulin, M. Kieffer, O. Didrit, and E. Walter, *Applied Interval Analysis*, vol. 66. London, U.K.: Springer-Verlag, 2001.
- [50] P. Casau, P. Rosa, and C. Silvestre, "Wind turbines fault detection and identification using set-valued observers," in *Proc. ACC*, 2012, pp. 4399–4404.
- [51] S. Skogestad and I. Postlethwaite, *Multivariable Feedback Control: Analysis and Design*, 2nd ed. New York, NY, USA: Wiley, 2005.
- [52] K. Zhou, J. Doyle, and K. Glover, *Robust Optimal Control*. Englewood Cliffs, NJ, USA: Prentice-Hall, 1996.
- [53] F. D. Bianchi, H. D. Battista, and R. J. Mantz, *Wind Turbine Control Systems*. New York, NY, USA: Springer-Verlag, 2007.
- [54] S. Heier, *Grid Integration of Wind Energy Conversion Systems*. New York, NY, USA: Wiley, 1998.
- [55] B. Boukhezzer, H. Siguerdidjane, and M. M. Hand, "Nonlinear control of variable-speed wind turbines for generator torque limiting and power optimization," *J. Solar Energy Eng.*, vol. 128, no. 4, pp. 516–530, 2006.
- [56] T. Esbensen and C. Sloth, "Fault diagnosis and fault-tolerant control of wind turbines," M.S. thesis, Dept. Electron. Syst., Aalborg Univ., Aalborg, Denmark, 2009.
- [57] R. Pena, J. C. Clare, and G. M. Asher, "Doubly fed induction generator using back-to-back PWM converters and its application to variable-speed wind-energy generation," *IEE Proc. Electr. Power Appl.*, vol. 143, no. 3, pp. 231–241, May 1996.
- [58] J. Jonkman, S. Butterfield, W. Musial, and G. Scott, "Definition of a 5-MW reference wind turbine for offshore system development," Nat. Renew. Energy Lab., Golden, CO, USA, Tech. Rep. NREL/TP-500-38060, Feb. 2009.
- [59] P. Young, "Controller design with mixed uncertainties," in *Proc. ACC*, Baltimore, Maryland, Jun. 1994, pp. 2333–2337.
- [60] P. Blue and S. Banda, "D-K iteration with optimal scales for systems with time-varying and time-invariant uncertainties," in *Proc. ACC*, Albuquerque, NM, USA, Jun. 1997, pp. 3967–3971.
- [61] S. Fekri, M. Athans, and A. Pascoal, "Robust multiple model adaptive control (RMMAC): A case study," *Int. J. Adapt. Control Signal Process.*, vol. 21, no. 1, pp. 1–30, 2006.
- [62] W. Rugh and J. Shamma, "A survey of research on gain-scheduling," *Automatica*, vol. 36, no. 10, pp. 1401–1425, 2000.
- [63] F. D. Bianchi, H. de Battista, and R. J. Mantz, "Wind turbine control systems: Principles, modelling and gain scheduling design," in *Advances in Industrial Control*. New York, NY, USA: Springer-Verlag, 2006.
- [64] I. Kaminer, A. M. Pascoal, P. P. Khargonekar, and E. E. Coleman, "A velocity algorithm for the implementation of gain-scheduled controllers," *Automatica*, vol. 31, no. 8, pp. 1185–1191, 1995.
- [65] C. Nichita, D. Luca, B. Dakyo, and E. Ceanga, "Large band simulation of the wind speed for real time wind turbine simulators," *IEEE Trans. Energy Convers.*, vol. 17, no. 4, pp. 523–529, Dec. 2002.
- [66] N. Laouti, N. Sheibat-Othman, and S. Othman, "Support vector machines for fault detection in wind turbines," in *Proc. 18th IFAC World Congr.*, Aug./Sep. 2011.
- [67] X. Zhang, Q. Zhang, S. Zhao, R. Ferrari, M. M. Polycarpou, and T. Parisini, "Fault detection and isolation of the wind turbine benchmark: An estimation-based approach," in *Proc. 18th IFAC World Congr.*, Aug./Sep. 2011.
- [68] A. A. Ozdemir, P. Seiler, and G. J. Balas, "Wind turbine fault detection using counter-based residual thresholding," in *Proc. 18th IFAC World Congr.*, Aug./Sep. 2011.
- [69] P. Casau and P. Rosa (2013). *Fitbox: Fault Identification Toolbox—A Wind Turbine Example* [Online]. Available: http://web.ist.utl.pt/~ist156338/fitbox/Wind_Turbine.zip



Pedro Casau received the B.Sc. and M.Sc. degrees in aerospace engineering from Instituto Superior Técnico, Lisbon, Portugal, in 2008 and 2010, respectively, where he is currently pursuing the Ph.D. degree in electrical and computer engineering.

He was a member of the Attitude Control Subsystem for the ESEO satellite from 2007 to 2009, where he was involved in the design of its control architecture. In 2011 and 2013, he was a Visiting Scholar with the University of Arizona, Tucson, AZ, USA. His current research interests include nonlinear control, hybrid control systems, vision-based control systems, and controller design for autonomous air vehicles.



Paulo Rosa received the Licenciatura degree and the Ph.D. degree in electrical and computer engineering from Instituto Superior Técnico (IST), Lisbon, Portugal, in 2006 and 2011, respectively.

He was a Post-Doctoral Researcher at IST. He was a Fault-Detection Specialist at Energias de Portugal, Lisbon, and is currently a Senior Project Engineer at Deimos Engenharia, Lisbon. His current research interests include robust adaptive control of LPV systems, guidance and control of autonomous vehicles, fault detection and isolation methods, and fault-tolerant control.



Seyed Mojtaba Tabatabaeipour received the Ph.D. degree in control and automation from Aalborg University, Aalborg, Denmark, in 2010.

He was with the Section for Automation and Control, Aalborg University, from 2010 to 2012, as a Post-Doctoral Researcher. He is currently a Post-Doctoral Researcher with the Section for Automation and Control, Department of Electrical Engineering, Technical University of Denmark, Kongens Lyngby, Denmark. His current research interests include fault diagnosis and fault-tolerant

control with application to energy systems.



Carlos Silvestre received the Licenciatura degree in electrical engineering, the M.Sc. degree in electrical engineering, the Ph.D. degree in control science, and the Habilitation degree in electrical engineering and computers from Instituto Superior Técnico (IST), Lisbon, Portugal, in 1987, 1991, 2000, and 2011, respectively.

He has been with the Department of Electrical Engineering, IST, since 2000, where he is currently an Associate Professor of Control and Robotics on leave. Since 2012, he has been an Associate

Professor with the Department of Electrical and Computers Engineering, Faculty of Science and Technology, University of Macau, Macau, China. Over the past years, he was involved in the research on the subjects of navigation guidance and control of air and underwater robots. His current research interests include linear and nonlinear control theory, coordinated control of multiple vehicles, gain-scheduled control, integrated design of guidance and control systems, inertial navigation systems, and mission control and real-time architectures for complex autonomous systems with applications to unmanned air and underwater vehicles.



Jakob Stoustrup (M'87–SM'99) received the M.Sc. degree in electrical engineering and the Ph.D. degree in applied mathematics from the Technical University of Denmark, Kongens Lyngby, Denmark, in 1987 and 1991, respectively.

He held several positions with the Department of Mathematics, Technical University of Denmark, from 1991 to 1996. He has been a Visiting Professor with the University of Strathclyde, Glasgow, U.K., and the Mittag-Leffler Institute, Stockholm, Sweden. From 1997 to 2013, he was a Professor of Automata

tion and Control with Aalborg University, Aalborg, Denmark, where he has been the Head of Research for the Department of Electronic Systems since 2006. Since 2014, he has been the Chief Scientist with the Pacific Northwest National Laboratory, Richland, WA, USA, where he is leading the Control of Complex Systems Initiative for the U.S. Department of Energy. He is involved in robust control theory and the theory of fault-tolerant control systems. He has proposed a novel plug-and-play control framework with coworkers. He has authored about 300 peer-reviewed scientific papers. Apart from the theoretical work, he has been involved in applications in cooperation with more than 100 industrial companies, including acting as the CEO for two technological startup companies.

Dr. Stoustrup has been an Associate Editor and Editorial Board Member of several international journals. He has served as the General Chair, Program Chair, and IPC Member of several international conferences. He has been the Chairman of the IEEE CSS/RAS Joint Chapter and the Vice Chair of the IEEE CSS Technical Committee on Smart Grids. In 2013, he was the first IEEE CSS Wikipedia Editor, the Chair of the IFAC Technical Committee SAFEPROCESS, and a member of IFAC Technical Board. He was a recipient of the Statoil Prize, the Dannin Award for Scientific Research, and several conference paper awards. He has been a member of the European Research Council, and the Danish, Norwegian, and Swedish Research Councils. He is a member of the Danish Academy of Technical Sciences, where he has been a Board Member.